0090-9556/04/3209-1040–1047$20.00
DRUG METABOLISM AND DISPOSITION

DMD 32:1040–1047, 2004

Vol. 32, No. 9
1417/1169877
Printed in U.S.A.

CARRIER-MEDIATED UPTAKE OF H_2-RECEPTOR ANTAGONISTS BY THE RAT CHOROID PLEXUS: INVOLVEMENT OF RAT ORGANIC ANION TRANSPORTER 3

Yoshinori Nagata, Hiroyuki Kusuhara, Shuichi Hirono, Hitoshi Endou, and Yuichi Sugiyama

Graduate School of Pharmaceutical Sciences, the University of Tokyo, Hongo, Bunkyo-ku, Tokyo, Japan (Y.N., H.K., Y.S.); School of Pharmaceutical Sciences, Kitasato University, Shirokane, Mitano-ku, Tokyo, Japan (S.H.); and Department of Pharmacology and Toxicology, Kyorin University School of Medicine, Shinkawa, Mitaka, Tokyo, Japan (H.E.)

Received February 17, 2004; accepted May 20, 2004

This article is available online at http://dmd.aspetjournals.org

ABSTRACT:

The choroid plexus (CP) acts as a site for the elimination of xenobiotic organic compounds from the cerebrospinal fluid (CSF). The purpose of the present study is to investigate the role of rat organic anion transporter 3 (rOat3; *Slc22a8*) in the uptake of H_2-receptor antagonists (cimetidine, ranitidine, and famotidine) by the isolated rat CP. Saturable uptake of cimetidine and ranitidine was observed in rOat3-LLC with K_m values of 80 and 120 μM, respectively, whereas famotidine was found to be a poor substrate. The steady-state concentration of the H_2-receptor antagonists in the CSF was significantly increased by simultaneously administered probenecid, although it did not affect their brain and plasma concentrations. Saturable uptake of cimetidine and ranitidine was observed in the isolated rat CP with K_m values of 93 and 170 μM, respectively, whereas 50% of the uptake of famotidine remained at the highest concentration examined (1 mM). The K_i value of ranitidine for the uptake of cimetidine by the isolated CP (50 μM) was similar to its own K_m value, suggesting that they share the same transporter for their uptake. The inhibition potency of organic anions such as benzylpenicillin, estradiol 17β-glucuronide, *p*-aminohippurate, and estrone sulfate for the uptake of cimetidine by the isolated rat CP was similar to that for benzylpenicillin, the uptake of which has been hypothesized to be mediated by rOat3, whereas a minimal effect by tetraethylammonium excludes involvement of organic cation transporter(s). These results suggest that rOat3 is the most likely candidate transporter involved in regulating the CSF concentration of H_2-receptor antagonists at the CP.

The choroid plexus (CP), located in the lateral, third, and fourth ventricles, is the site of production of cerebrospinal fluid (CSF) (Segal, 2000; Haselbach et al., 2001). It is well established that CP acts as a barrier between the CSF and the circulating blood, and it is referred to as the blood-CSF barrier (Suzuki et al., 1997; Ghersi-Egea and Strazielle, 2001; Haselbach et al., 2001; Kusuhara and Sugiyama, 2001). The barrier function is achieved partly by the tight monolayer of choroid plexus epithelial cells and partly by detoxification systems consisting of metabolic enzymes and multispecific transporters (Suzuki et al., 1997; Ghersi-Egea and Strazielle, 2001; Haselbach et al., 2001; Kusuhara and Sugiyama, 2001).

Histamine H_2-receptor antagonists have been used clinically to cure duodenal ulcers and gastric acid hypersecretion, and adverse effects by H_2-receptor antagonists on the central nervous system, ranging from mild dizziness, restlessness, and mental confusion to advanced symptoms such as myoclonic twitching and seizure, have been reported (Grimson, 1977; Schentag et al., 1979; McGuigan, 1981). Schentag et al. (1979) reported that the concentration of cimetidine in the CSF is related to the mental status. We demonstrated previously that a saturable mechanism is involved in the elimination of cimetidine from the CSF after intracerebroventricular administration (Suzuki et al., 1985, 1988). Transport studies revealed that the uptake of cimetidine by the isolated rat choroid plexus is saturable, and the efflux transport across the CP has been considered to account for the saturable elimination mechanism of cimetidine from the CSF (Suzuki et al., 1986). Organic anions such as benzylpenicillin and *p*-aminohippurate (PAH) inhibit the uptake of cimetidine by the isolated rat choroid plexus, whereas organic cations such as tetraethylammonium (TEA) and *N*-methylnicotinamide have no such effect (Suzuki et al., 1986). It is likely that organic anion transporter(s) play a major role in regulating the CSF concentration of cimetidine at the CP.

We have isolated rat organic anion transporter 3 (rOat3; *Slc22a8*), the third isoform of the Oat/OAT family, from the rat brain cDNA library by homology cloning (Kusuhara et al., 1999). Functional expression of rOat3 in *Xenopus laevis* oocytes and mammalian cells has revealed its broad substrate specificity for organic anions, including PAH and benzylpenicillin (Kusuhara et al., 1999; Burckhardt and Burckhardt, 2003; Dantzler and Wright, 2003). In the CP, although mRNA expression of all the Oat isoforms (rOat1~rOat3) has been detected (Sweet et al., 2002; Choudhuri et al., 2003), rOat3 is the most abundant isoform (Choudhuri et al., 2003). rOat3 has been shown to be expressed on the brush border membrane of the CP (Nagata et al., 2002). Localization of rOat3 in the CP suggests its involvement in the uptake process at the CP. Since the spectrum of inhibitors and kinetic

This work was supported by grant-in-aids from the Ministry of Health, Labor and Welfare of Japan and a grant-in-aid for Scientific Research (B) (KAKENHI 15390035).

ABBREVIATIONS: CP, choroid plexus; CSF, cerebrospinal fluid; PAH, *p*-aminohippurate; TEA, tetraethylammonium; Oat, organic anion transporter; MEP, molecular electrostatic potential(s); LC-MS, liquid chromatography-mass spectometry; Oct, organic cation transporter.

parameters for the uptake of PAH and benzylpenicillin by the isolated rat CP were similar to those for rOat3, it has been hypothesized that rOat3 accounts for their uptake by the isolated rat CP (Nagata et al., 2002). Furthermore, the finding that the isolated choroid plexus from mOat3 knockout mice was unable to cellularly accumulate fluorescein supports the role of Oat3 in the CP (Sweet et al., 2002). H_2-receptor antagonists have been referred to as bisubstrates recognized by both renal organic anion and cation transporters (Ullrich et al., 1993). Indeed, cimetidine is a substrate of rOat3 as well as organic cation transporter(s) (Grundemann et al., 1999; Kusuhara et al., 1999). Therefore, it is likely that rOat3 plays a major role in the uptake of cimetidine and other H_2-receptor antagonists by the isolated rat CP.

The primary purpose of the present study was to investigate the importance of rOat3 in regulating the concentration of H_2-receptor antagonists (cimetidine, ranitidine, and famotidine). We examined whether ranitidine and famotidine are substrates of rOat3 in LLC-PK1 cells expressing rOat3 (rOat3-LLC). rOat3-LLC exhibits specific uptake of ranitidine and famotidine, but the transport activity of famotidine was quite low compared with that of cimetidine and ranitidine. Steady-state concentrations of H_2-receptor antagonists in the CSF and plasma were determined in rats treated with or without probenecid, a potent inhibitor of rOat3. The uptake of H_2-receptor antagonists was investigated using the isolated rat CP, and the kinetic parameters and spectrum of inhibitors were compared with those for benzylpenicillin.

Materials and Methods

Materials. [^{3}H]Cimetidine (16.5 Ci/mmol) and [^{14}C]urea (52 mCi/mmol) were purchased from Amersham Biosciences UK, Ltd. (Little Chalfont, Buckinghamshire, UK). All cell culture media and reagents were obtained from Invitrogen (Carlsbad, CA), except fetal bovine serum (Cansera International Inc., Ontario, Canada). All other chemicals and reagents were of analytical grade and readily available from commercial sources.

Calculation of Molecular Electrostatic Potential (MEP) of H_2-Receptor Antagonists. The starting structures of H_2-receptor antagonists were built up on the basis of standard bond lengths and angles, and the structures of H_2-receptor antagonists were optimized using the AM1 Hamiltonian and conductor-like screening model. Their molecular electrostatic potentials at pH 7.4 were calculated using the modified neglect of diatomic overlap Hamiltonian. All calculations were carried out by the MOPAC97 (CS Chem3D Pro; CambridgeSoft Corporation, Cambridge, MA).

Uptake Studies by rOat3-LLC. rOat3-LLC was established previously, and all the procedures have been described in detail (Sugiyama et al., 2001). Cells were seeded on a 12-well dish (BD Biosciences, Franklin Lakes, NJ) at a density of 1.2×10^5 cells/well and cultured for 3 days. Sodium butyrate (5 mM) was added to the culture medium to induce expression of the transporter 24 h before starting the experiments (Sugiyama et al., 2001). Uptake was initiated by adding medium containing ligands, with or without inhibitors, after the cells had been washed twice and preincubated with Krebs-Henseleit buffer at 37°C for 15 min. This buffer consists of 142 mM NaCl, 23.8 mM Na_2CO_3, 4.83 mM KCl, 0.96 mM KH_2PO_4, 1.20 mM $MgSO_4$, 12.5 mM HEPES, 5 mM glucose, and 1.53 mM $CaCl_2$ adjusted to pH 7.4. The uptake was terminated at a designated time by adding ice-cold Krebs-Henseleit buffer. For [^{3}H]cimetidine uptake, cells were dissolved in 500 μl of 1 N NaOH, kept overnight, neutralized with 250 μl of 2 N HCl, and then aliquots (500 μl) were transferred to scintillation vials. The radioactivity associated with the cells and medium was determined in a liquid scintillation spectrophotometer (LS6000SE; Beckman Coulter, Fullerton, CA) after adding scintillation fluid (Hionic-Fluor; PerkinElmer Life and Analytical Sciences, Boston, MA) to the vials. For the determination of the uptake of ranitidine and famotidine, cells were dissolved in 200 μl of 0.2 N NaOH, and aliquots (50 μl) were used for LC-MS quantification as described below. The remaining portions of cell lysate were used to determine the protein concentration by the method of Lowry, with bovine serum albumin as a standard. Ligand uptake was given as the cell-to-medium concentration ratio determined as the amount of ligand associated with cells divided by the medium concentration.

Uptake Studies by Isolated Rat CP. Male Sprague-Dawley rats weighing 250 to 300g were purchased from SLC (Shizuoka, Japan). The CP was isolated from the lateral ventricles and incubated at 37°C for 1 min in 500 μl of artificial CSF, which consists of 122 mM NaCl, 25 mM $NaHCO_3$, 10 mM glucose, 3 mM KCl, 1.4 mM $CaCl_2$, 1.2 mM $MgSO_4$, 0.4 mM K_2HPO_4, and 10 mM HEPES (pH 7.3), equilibrated with 95% O_2/5% CO_2. Radiolabeled ligands, with or without inhibitors, were added simultaneously to initiate uptake. The uptake of [^{3}H]cimetidine and [^{14}C]TEA by isolated rat CP was examined by centrifugal filtration as described previously (Nagata et al., 2002). The tissue-to-medium concentration ratio of [^{3}H]cimetidine and [^{14}C]TEA was calculated with [^{14}C]urea or [^{3}H]water as a cell water space marker and corrected for the adherent water space. The ^{3}H and ^{14}C activity in the specimens was determined in a liquid scintillation spectrophotometer. To determine the uptake of nonradiolabeled H_2-receptor antagonists, the rapid filtration method was used since the silicon oil, used in the centrifugal filtration method, disturbed the quantification by LC-MS. The uptake of cimetidine, ranitidine, and famotidine by isolated rat CP was terminated by rapid filtration using a vacuum manifold; then the CP was rinsed three times with 300 μl of artificial CSF, the CP was dissolved in 100 μl of 0.2 N NaOH, and aliquots (50 μl) were subjected to LC-MS quantification as described below. The remaining portions of lysate were used to determine the protein concentration by the method of Lowry, with bovine serum albumin as a standard.

Constant Infusion Study in Rats. Rats were lightly anesthetized with ether, and the left femoral vein was cannulated with polyethylene tubing (PE-50; BD Biosciences). The priming dose of the H_2 antagonist and probenecid was 2 and 15 mg/kg, respectively. The H_2 antagonist and probenecid were given to rats through the femoral vein cannula at 2 and 30 mg/h/kg, respectively, for 3 h. The dose regimen was designed to obtain a CSF concentration of probenecid sufficient to inhibit rOat3. Blood samples (300 μl) were collected from the tail vein at 1 and 2 h during the infusion. At the end of the experiment, blood samples were collected from the abdominal vein, and animals were sacrificed by bleeding the abdominal aorta under ether anesthesia. Following sacrifice, 50- to 100-μl aliquots of CSF were obtained by cisternal puncture using insulin syringes (0.5-ml syringe with a 29-gauge × 1/2-inch attached needle; TERUMO Corporation, Tokyo, Japan), and whole brains were removed and weighed. To obtain plasma, blood was centrifuged at 10,000g for 5 min. For determination of the unbound plasma concentration, aliquots (0.5 ml) of plasma specimens were subjected to filtration (2500 rpm, 10 min) (MPS-1; Millipore Corporation, Bedford, MA). The brain samples were homogenized in three volumes of water using a Polytron homogenizer (Brinkmann Instruments, Westbury, NY). The concentrations of H_2-receptor antagonists and probenecid in plasma, plasma ultrafiltrate, and brain homogenate were quantified by LC-MS as described below.

Quantification of H_2-Receptor Antagonists and Probenecid by LC-MS. The quantification of cimetidine, ranitidine, famotidine, and probenecid was performed by a high-performance liquid chromatograph (Alliance 2690; Waters, Milford, MA) connected to a mass spectrometer (ZMD; Micromass UK Ltd., Manchester, UK). Aliquots (50 μl) of samples containing H_2-receptor antagonists were precipitated by adding 100 μl of methanol containing an internal standard (famotidine for cimetidine and ranitidine and cimetidine for famotidine), mixed, and centrifuged, and 20 μl of the supernatants was subjected to LC-MS. Aliquots (50 μl) of samples containing probenecid were precipitated by adding 100 μl methanol, mixed, and centrifuged, and aliquots (10 μl) of the supernatants were diluted with 990 μl of methanol, 20 μl of which was subjected to LC-MS. High-performance liquid chromatography analysis was performed on an Waters Xterra MS C18 column (2.5 μm, 3 mm i.d., 30 mm) at room temperature. Elution was performed with a 0 to 100% linear gradient of 10 mM ammonium acetate/methanol over 4 min at 0.8 ml/min. A portion of the eluent (split ratio = 1:3) was introduced into the MS via an electrospray interface. Detection was performed by selective ion monitoring in positive ion mode (m/z: 253, 315, 338, and 286 for cimetidine, ranitidine, famotidine, and probenecid, respectively).

Kinetic Analyses. Kinetic parameters were obtained using the Michaelis-Menten equation $v = V_{max} \times S/(K_m + S) + P_{dif} \times S$, where v is the uptake rate of the substrate (pmol/min/mg protein or pmol/min/μl tissue), S is the substrate concentration in the medium (μM), K_m is the Michaelis-Menten constant (μM), and V_{max} is the maximum uptake rate (pmol/min/mg protein or pmol/min/μl tissue). P_{dif} represents the uptake clearance corresponding to the

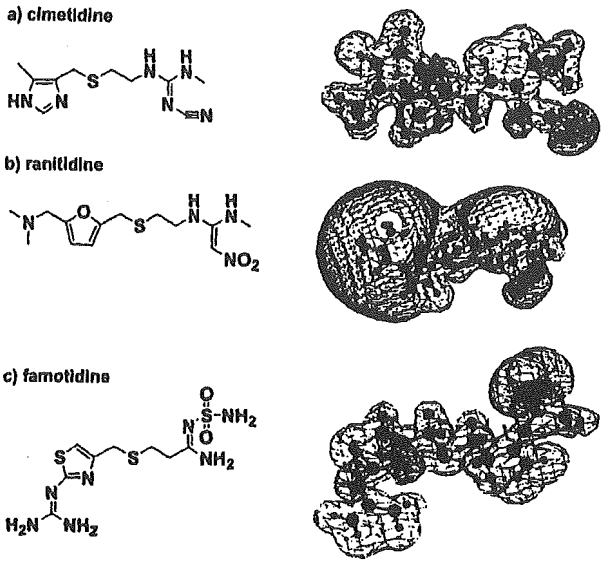

FIG. 1. Molecular structures and molecular electrostatic potential of H_2-receptor antagonists. MEP of cimetidine, ranitidine, and famotidine at pH 7.4 were calculated using the MNDO Hamiltonian. The figure illustrates the isoelectric line at 2.8 atomic units. The colors indicate the charge of their electrostatic potential: red is positive and blue is negative.

nonsaturable component (μl/min/mg protein or μl/min/μl tissue). To obtain the kinetic parameters, the equation was fitted to the uptake velocity using a MULTI program (Yamaoka et al., 1981). The input data were weighted as the reciprocals of the observed values, and the Damping Gauss-Newton method algorithm was used for fitting. Inhibition constants (K_i) were calculated by assuming competitive inhibition using the equation $CL_{+inh} = CL/(1 + I/K_i) + P_{diff}$ where CL_{+inh} represents the uptake clearance and $_{+inh}$ represents the value in the presence of inhibitor. I represents the concentration of inhibitor (μM). The substrate concentration was low compared with its K_m value in the inhibition study.

Results

Molecular Electrostatic Potential of H_2-Receptor Antagonists. Figure 1 illustrates the chemical structures of the H_2-receptor antagonists and their isoelectric lines at 2.8 atomic units calculated at pH 7.4. There was a region showing negative MEP in the chemical structures of H_2-receptor antagonists (Fig. 1; indicated by blue in the cyanoimine group for cimetidine, the nitro group for ranitidine, and the imine and sulfonamide groups for famotidine).

Uptake of H_2-Receptor Antagonists (Cimetidine, Ranitidine, and Famotidine) by rOat3-LLC. Figure 2 shows the time profiles of the uptake of cimetidine, ranitidine, and famotidine by vector- and rOat3-LLC. The uptake of cimetidine, ranitidine, and famotidine was significantly greater in rOat3-LLC than in vector-LLC, although the absolute value of famotidine uptake was quite small compared with that of cimetidine and ranitidine (Fig. 2). For further analyses, the uptake of cimetidine and ranitidine was determined at the earliest time, both technically and practically (3 min for cimetidine and 5 min for ranitidine). The uptake of cimetidine and ranitidine was saturable (Fig. 3), and kinetic analyses revealed that the K_m and V_{max} values of cimetidine and ranitidine by rOat3-LLC were 79.2 ± 17.8 and 121 ± 36 μM and 150 ± 29 and 367 ± 95 pmol/min/mg protein, respectively. The uptake clearance corresponding to the saturable component (V_{max}/K_m) for cimetidine and ranitidine was 1.89 ± 0.30 and 3.03 ± 0.39 μl/min/mg protein, respectively, whereas that corresponding to the nonsaturable component was 1.07 ± 0.03 and 0.381 ± 0.023 μl/min/mg protein, respectively.

Effect of Organic Anions and Cations on the Uptake of Cimetidine by rOat3. Benzylpenicillin and ranitidine inhibited the rOat3-mediated [^{3}H]cimetidine uptake in a concentration-dependent manner (Fig. 4, a and b), whereas TEA had no inhibitory effect at the concentrations examined (0.1 to 10 mM; data not shown). The K_i values of benzylpenicillin and ranitidine for cimetidine uptake by rOat3-LLC were determined to be 76.7 ± 13.2 and 119 ± 44 μM, respectively. Famotidine only weakly inhibited the uptake of cimetidine by rOat3-LLC (Fig. 4c).

Effect of Probenecid on the Plasma, Brain, and CSF Concentrations of H_2-Receptor Antagonists. Rats were given H_2-receptor antagonists by constant infusion with or without probenecid. The plasma concentrations of H_2-receptor antagonists reached steady-state within 3 h (data not shown), whereas the plasma concentration of probenecid showed a gradual increase during infusion (355 ± 107 μM at 1 h, 514 ± 143 μM at 2 h, and 651 ± 246 μM at 3h). The unbound plasma concentration and CSF concentration of probenecid at 3 h were 154 ± 26 and 57.3 ± 2.0 μM, respectively. Probenecid treatment did not affect the brain and plasma concentrations of the H_2-receptor antagonists (Table 1), whereas their CSF concentrations significantly increased (Table 1). The CSF-to-unbound plasma concentration ratio ($C_{CSF}/C_{p,fu}$) significantly increased by 3.7-fold for cimetidine, 4.3-fold for ranitidine, and 2.5-fold for famotidine (Table 1).

Uptake of H_2-Receptor Antagonists by the Isolated Rat CP. The time profiles of the uptake of [^{3}H]cimetidine and [^{14}C]TEA by isolated rat CP are shown in Fig. 5a (uptake units: μl/μl CP volume) and those of cimetidine, ranitidine, and famotidine are shown in Fig. 5b (uptake units: μl/mg protein). All the H_2-receptor antagonists showed time-dependent accumulation by the isolated rat CP, and their transport activities were in the following order: ranitidine ≈ cimetidine > famotidine (Fig. 5b). The uptake of TEA by the isolated rat CP was small compared with that of H_2-receptor antagonists (Fig. 5a). The uptake of [^{3}H]cimetidine and ranitidine was saturable, and kinetic analyses revealed that the uptake of [^{3}H]cimetidine and ranitidine consists of one saturable and one nonsaturable component (Fig. 6). The K_m and V_{max} values and uptake clearance corresponding to the nonsaturable component of [^{3}H]cimetidine were 92.7 ± 46.1 μM, 137 ± 71 pmol/min/μl tissue, and 0.581 ± 0.123 μl/min/μl tissue, respectively, whereas the corresponding values for ranitidine were 171 ± 57 μM, 1250 ± 360 pmol/min/mg protein, and 1.49 ± 0.26 μl/min/mg protein. The uptake of famotidine was saturated at high substrate concentrations (Table 2), but 50% of the total uptake remained at the highest concentration examined (1 mM, Table 2).

Effect of Organic Anions and TEA on the Uptake of Cimetidine by Isolated Rat CP. The effect of benzylpenicillin and TEA was examined with regard to the uptake of cimetidine, ranitidine, and famotidine by the isolated rat CP (Table 2). Benzylpenicillin inhibited the uptake of the H_2-receptor antagonists in a concentration-dependent manner. TEA did not affect the uptake of H_2-receptor antagonists. Furthermore, the effect of estradiol-17β-glucuronide, estrone sulfate, benzylpenicillin, PAH, ranitidine, and famotidine was also examined with regard to the uptake of [^{3}H]cimetidine by isolated rat CP (Fig. 7). All organic anions, ranitidine, and famotidine showed a concentration-dependent inhibition of the uptake of [^{3}H]cimetidine by the isolated rat CP (Fig. 7), and their inhibition constants are summarized in Table 3. The K_i and K_m values for the uptake of benzylpenicillin and cimetidine by the isolated rat CP were comparable (Table 3).

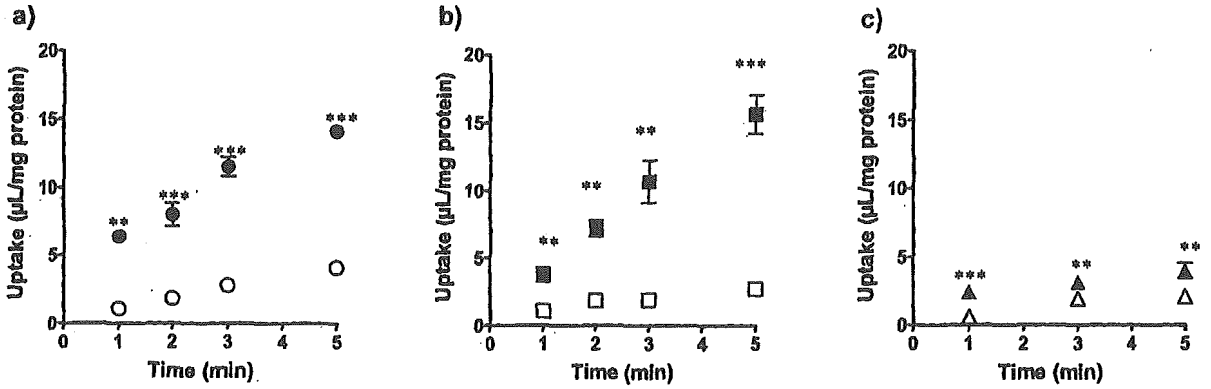

FIG. 2. Uptake of cimetidine, ranitidine, and famotidine by rOat3-LLC. The uptake of [^{3}H]cimetidine (a; circle), ranitidine (b; square) and famotidine (c; triangle) by rOat3-LLC (closed symbol) and vector-LLC (open symbol) was determined. The uptake was initiated by adding ligand ([^{3}H]cimetidine (1 μM), ranitidine (10 μM), and famotidine (10 μM) and terminated at designated times by adding ice-cold buffer. Each point represents the mean ± S.E. (n = 3–6). **, $p < 0.01$ and ***, $p < 0.001$, significantly different from vector-LLC (unpaired t test).

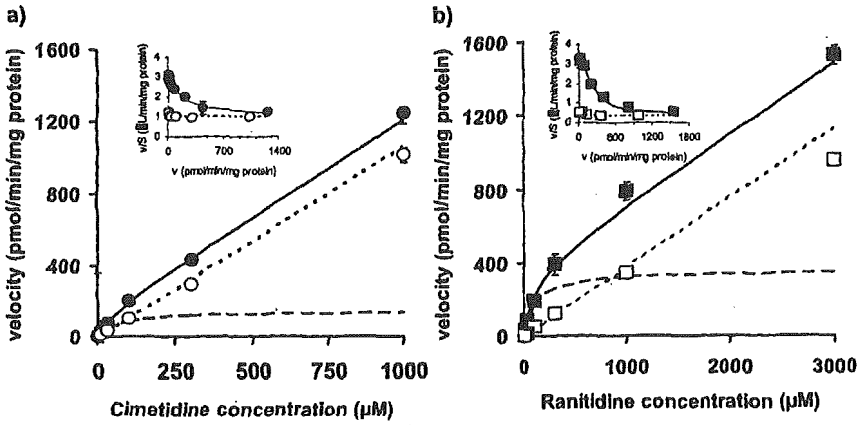

FIG. 3. Concentration dependence of the uptake of cimetidine and ranitidine by rOat3-LLC. The cellular accumulation of [^{3}H]cimetidine (a) and ranitidine (b) by rOat3-LLC for 3 and 5 min was determined at different substrate concentrations. The concentration dependence of the uptake of cimetidine and ranitidine by rOat3-LLC is shown as Eadie-Hofstee plots in the inset. Kinetic analyses revealed that the uptake of [^{3}H]cimetidine and ranitidine consists of one saturable and one nonsaturable component and follows the Michaelis-Menten equation. The solid, dotted, and broken lines represent the fitted line, the clearance of the nonsaturable component, and the clearance of the saturable component obtained by nonlinear regression analysis, respectively. Each point represents the mean ± S.E. (n = 3–6).

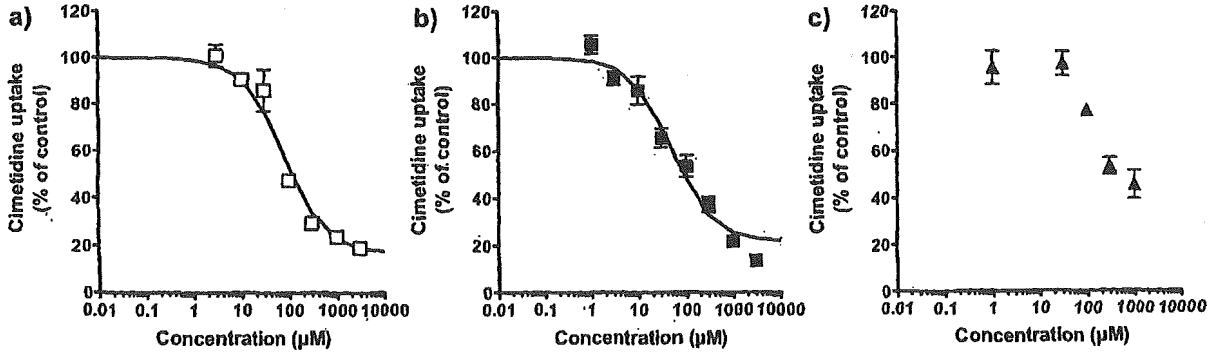

FIG. 4. Effect of organic anions and cations on the uptake of cimetidine by rOat3. The cellular accumulation of [^{3}H]cimetidine (1 μM) by rOat3 for 3 min was determined in the presence and absence of nonradiolabeled compounds at the concentrations indicated. Symbols represent benzylpenicillin (a; □), ranitidine (b; ■), and famotidine (c; ▲). The inhibition constants (K_i) of these compounds were calculated by assuming competitive inhibition. The solid lines represent the fitted line obtained by nonlinear regression analysis. The details of the fitting are described under *Materials and Methods*. Each point represents the mean ± S.E. (n = 3).

Discussion

In the present study, we reported that rOat3 is involved in the uptake of H_2-receptor antagonists (cimetidine, ranitidine, and famotidine) by the isolated rat CP, and that drug-drug interaction causes an increase in the CSF concentration of H_2-receptor antagonists without affecting their plasma concentration. rOat3 has been characterized by

TABLE 1

Total plasma, unbound plasma, CSF, and brain concentrations of H_2-receptor antagonists after intravenous infusion in rats treated with or without probenecid

H_2-receptor antagonists (2 mg/kg) were administered to rats by bolus intravenous administration followed by constant infusion (2 mg/h/kg) during 3 h. Probenecid (15 mg/kg) was administered to rats by bolus intravenous administration followed by constant infusion (30 mg/h/kg) during 3 h, and the unbound plasma concentrations and CSF concentrations of probenecid at 3 h were 154 ± 26 and 57.3 ± 2.0 μM, respectively. Each value represents the mean ± S.D. (n = 3).

	Cimetidine		Ranitidine		Famotidine	
	Control	+Probenecid	Control	+Probenecid	Control	+Probenecid
C_p (μM)	3.71 ± 1.20	2.97 ± 0.15	2.65 ± 1.25	2.11 ± 0.18	3.47 ± 1.22	2.79 ± 0.03
$C_{p,fu}$ (μM)	2.25 ± 0.60	1.89 ± 0.11	1.72 ± 0.49	1.52 ± 0.06	2.01 ± 0.72	1.54 ± 0.18
C_{CSF} (nM)	39.1 ± 19.8	116 ± 17**	25.9 ± 12.0	97.1 ± 5.2***	23.1 ± 9.2	43.9 ± 4.1*
C_{brain} (nM)	96.5 ± 27.1	99.9 ± 12.5	85.7 ± 33.8	83.9 ± 10.9	106 ± 30	102 ± 18
$C_{CSF}/C_{p,fu}$ ratio	0.0166 ± 0.005	0.0615 ± 0.0121**	0.0147 ± 0.0046	0.0639 ± 0.0046***	0.0114 ± 0.0027	0.0289 ± 0.0057**

C_p, total plasma concentration; $C_{p,fu}$, unbound plasma concentration; C_{CSF}, CSF concentration; C_{brain}, brain concentration.
* $p < 0.05$, ** $p < 0.01$, and *** $p < 0.001$, significantly different from control rats (unpaired t test).

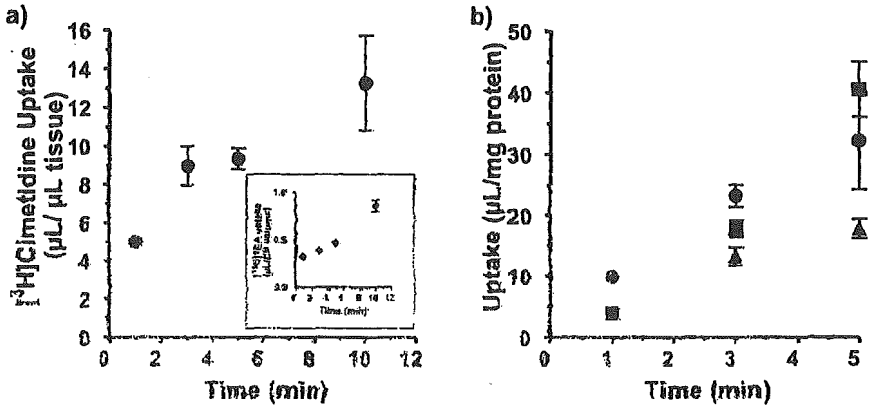

FIG. 5. Uptake of cimetidine, ranitidine, famotidine, and TEA by the isolated rat CP. The rat CP was isolated from the lateral ventricles. a, uptake of [^{3}H]cimetidine (●) and [^{14}C]TEA (◆) by the isolated rat CP was determined by the centrifugal filtration method as described under *Materials and Methods*. The tissue-to-medium concentration ratio of [^{3}H]cimetidine and [^{14}C]TEA was calculated with [^{14}C]urea and [^{3}H]water as cell water space markers, respectively, and corrected for the adherent water space. b, uptake of cimetidine (10 μM; ●), ranitidine (10 μM; ■), and famotidine (10 μM; ▲) by the isolated CP was determined by the rapid filtration method followed by quantification using LC-MS. Each point represents the mean ± S.E. (n = 3).

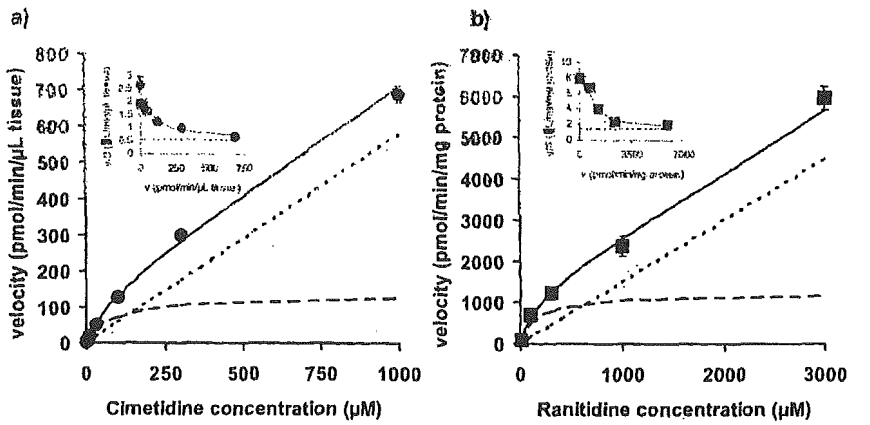

FIG. 6. Concentration dependence of cimetidine and ranitidine accumulation by the isolated rat CP. The accumulation of [^{3}H]cimetidine (a) and ranitidine (b) in the isolated rat CP for 3 and 5 min, respectively, was determined at various substrate concentrations. The concentration dependence for the uptake of [^{3}H]cimetidine and ranitidine is shown as Eadie-Hofstee plots in the inset. Kinetic analyses revealed that the uptake of [^{3}H]cimetidine and ranitidine consists of one saturable and one nonsaturable component and follows the Michaelis-Menten equation. The solid, dotted, and broken lines represent the fitted line, the clearance of the nonsaturable component, and the clearance of the saturable component obtained by nonlinear regression analysis, respectively. Each point represents the mean ± S.E. (n = 3).

its broad substrate specificity for organic anions, from amphipathic to hydrophilic organic anions, and also a weakly basic compound, cimetidine (Kusuhara et al., 1999). In addition to cimetidine, ranitidine was found to be a good substrate of rOat3, whereas famotidine seems to be a poor substrate of rOat3 (Fig. 2). Because it is one of the clues to understanding the interaction of such weak base or cationic compounds with rOat3, the MEP of the H_2-receptor antagonists was calculated (Fig. 1). The H_2-receptor antagonists contain a region of

TABLE 2

Effect of benzylpenicillin and TEA on the uptake of H_2-receptor antagonists by the isolated rat CP

The uptake of cimetidine, ranitidine, and famotidine by isolated rat CP was determined in the presence and absence of benzylpenicillin and TEA at the concentrations indicated. The substrate concentration of cimetidine, ranitidine, and famotidine was 10 μM, and the excess amount of unlabeled substrates represents concentrations of 3, 3, and 1 mM for cimetidine, ranitidine, and famotidine, respectively. Each value represents the mean ± S.E. (n = 3).

	Concentration	Uptake (Percentage of Control)		
		Cimetidine	Ranitidine	Famotidine
	mM			
Control		100 ± 7	100 ± 12	100 ± 22
Excess cold		30.4 ± 1.1	24.8 ± 1.1	50.5 ± 3.6
Benzylpenicillin	0.1	72.5 ± 5.1	76.7 ± 19	83.8 ± 8.3
	1	46.3 ± 1.1	34.9 ± 3.9	78.6 ± 6.6
	3	30.4 ± 1.1	31.8 ± 3.5	51.6 ± 1.9
TEA	0.1	99.5 ± 8.3	94.8 ± 14	120 ± 3
	1	87.5 ± 6.1	97.3 ± 8.6	110 ± 14
	3	93.7 ± 10.5	88.8 ± 13.6	93.4 ± 3.6

negative MEP in their chemical structures (Fig. 1). As Ullrich et al. (1993) suggested, this site might play a key role for the substrate recognition of H_2-receptor antagonists by rOat3. Suzuki et al. (1987) clearly demonstrated a linear correlation between the lipophilicity and reciprocal number of K_i values of β-lactam antibiotics for the uptake of benzylpenicillin by the isolated rat CP. Lipophilicity is likely to be an important factor for recognition by rOat3 in the case of β-lactam antibiotics. In contrast, the kinetic parameters of cimetidine and ranitidine for their uptake by rOat3 were comparable, although they had different cLogD values. Lipophilicity may not be a determinant factor in the case of the H_2-receptor antagonists.

Probenecid has previously been reported to inhibit the apical-to-basal side of azidodeoxythymidine (corresponding to the efflux transport from the CSF side to the blood side under physiological conditions), resulting in an increase in the basal-to-apical transport (Strazielle et al., 2003). Simultaneous administration of probenecid caused a significant increase in the CSF concentration of all the H_2-receptor antagonists examined (Table 1). Since it did not affect the brain and unbound plasma concentrations, it is likely that the effect of probenecid is due to the inhibition of the efflux transport of H_2-receptor antagonists across the CP (Table 1). Strazielle et al. (2003) also found that benzbromarone had an inhibitory effect for the apical-to-basal transport of azidodeoxythymidine. It is possible that benzbromarone treatment also causes an increase in the CSF concentration of H_2-receptor antagonists. Since the brain-to-unbound plasma concentration ratio of the H_2-receptor antagonists was well below unity (Table 1), it is possible that the efflux transport across the brain capillaries limits their brain distribution; however, probenecid had no effect on the brain concentration. Further studies are necessary to investigate whether the H_2-receptor antagonists undergo the efflux across the brain capillaries and whether organic anion transporters, including rOat3, contribute to this efflux.

The uptake, an initial process for elimination from the CSF, was investigated using the isolated rat CP. Time-dependent uptake of the H_2-receptor antagonists was detected in the isolated rat CP (Fig. 5). The saturable component accounts for a large part of the total uptake of cimetidine and ranitidine (Fig. 6). The uptake of cimetidine by the isolated rat CP was markedly inhibited by benzylpenicillin with a K_i value similar to its own K_m value for uptake by the isolated rat CP (Nagata et al., 2002). Conversely, the K_m value of cimetidine for the uptake by the isolated rat CP was similar to its K_i value for the uptake

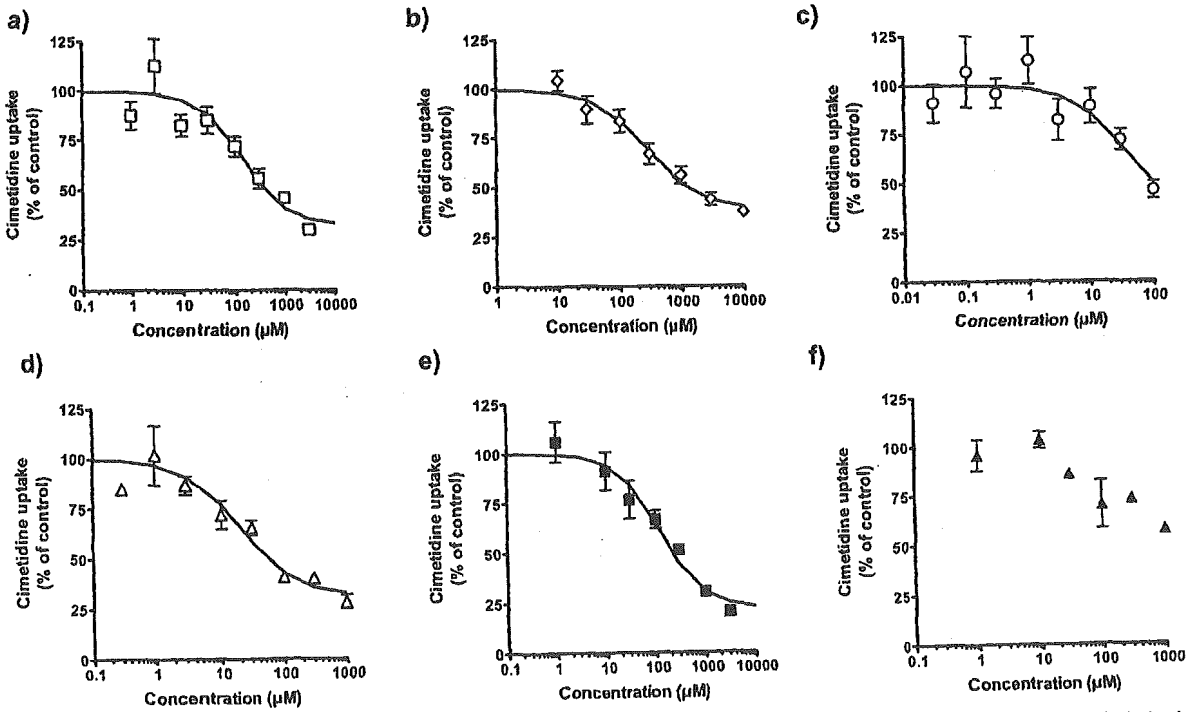

FIG. 7. Inhibitory effect of organic anions and cations on the uptake of cimetidine by the isolated rat CP. The accumulation of [^{3}H]cimetidine (1 μM) by the isolated rat CP for 3 min was determined in the presence and absence of nonradiolabeled compounds at the concentrations indicated. Symbols represent benzylpenicillin (a; □), PAH (b; ◇), estradiol-17β-glucuronide (c; ○), estrone sulfate (d; △), ranitidine (e; ■), and famotidine (f; ▲). The solid lines represent the fitted line obtained by nonlinear regression analysis. The details of the fitting are described under *Materials and Methods*. Each point represents the mean ± S.E. (n = 3).

TABLE 3

K_i and K_m values for the uptake of cimetidine, ranitidine, and benzylpenicillin by the isolated rat CP

The effect of estrone sulfate, cimetidine, estradiol-17β-glucuronide ($E_2$17βG), PAH, benzylpenicillin, and ranitidine was examined with regard to uptake by the rat isolated CP. The K_i and K_m values were determined by nonlinear regression analysis as described under *Materials and Methods*. Data are taken from Fig. 7. Each value represents the mean ± S.E. (n = 3–6).

	K_i and K_m values (μM)		
	Benzylpenicillin[a]	Cimetidine	Ranitidine
Estrone sulfate	22.3	19.5 ± 8.8	
Cimetidine	44.4	92.7 ± 46.1[b]	
$E_2$17βG	33.0	36.3 ± 15.7	
PAH	406	281 ± 74	
Benzylpenicillin	111[b]	140 ± 97	
Ranitidine		49.6 ± 15.1	171 ± 57[b]

[a] Parameters cited from Nagata et al. (2002).
[b] K_m value.

of benzylpenicillin by the isolated CP (Table 3; Nagata et al., 2002). Furthermore, the inhibition constants of the compounds listed in Table 3, which are substrates of rOat3, are similar for the uptake of cimetidine and benzylpenicillin by the isolated rat CP (Table 3). These results suggest that the same organic anion transporter, namely, rOat3, is responsible for the uptake of cimetidine by the isolated rat CP. Since the K_i value of ranitidine for the uptake of cimetidine was close to its K_m value (Table 3) and benzylpenicillin showed similar inhibition potency (Table 2), rOat3 is presumably also involved in the uptake of ranitidine. Since the uptake of famotidine was saturable and inhibited by benzylpenicillin (Table 2), the involvement of a transporter was suggested, although the fraction of the saturable component could not be precisely estimated due to its limited solubility. This is consistent with the in vivo result. Since famotidine is a poor substrate of rOat3, the benzylpenicillin-sensitive fraction of famotidine uptake may at least partly be accounted for by rOat3; however, it is possible that other transporters distinct from rOat3 and organic cation transporter may play a major role in the uptake of famotidine by the isolated rat CP. Villalobos et al. (1997) demonstrated the presence of a membrane potential-sensitive uptake mechanism for hydrophilic organic cations at the primary cultured CP epithelial cells. Reverse transcription-polymerase chain reaction analyses detected mRNA expression of Oct2 and Oct3 in the CP, and this may account for the uptake of hydrophilic organic cations in the CP (Sweet et al., 2001). The expression level of rOct2 in the CP was considerably lower than that in the kidney, whereas that of rOct3 was the same for all the tissues examined, although the absolute value was low (Choudhuri et al., 2003). The low expression of Oct mRNA may account for the lower uptake of TEA by the isolated rat CP compared with that of the H_2-receptor antagonists (Fig. 5). Although cimetidine is a substrate of rOct2 (Grundemann et al., 1999), the effect of TEA on the uptake of the H_2-receptor antagonists by the isolated rat CP was minimal, even at a concentration sufficient to saturate TEA uptake by primary cultured choroid epithelial cells (Table 2) (Villalobos et al., 1997). Therefore, the contribution of rOcts to the total uptake of H_2-receptor antagonists by the isolated rat CP is minimal, although they are involved.

rOat3 has been shown to be expressed on the basolateral membrane of the proximal tubules and involved in the uptake of organic anions (Hasegawa et al., 2002, 2003). However, probenecid treatment did not affect the steady-state plasma concentration of H_2-receptor antagonists, although the unbound plasma concentration was sufficient to inhibit rOat3-mediated uptake (Table 1). This result is in a good agreement with the previous report by Boom and Russel (1993). They examined the uptake of cimetidine by freshly isolated rat proximal tubular cells and demonstrated that the major fraction of cimetidine uptake (approximately 50%) was inhibited by TEA (Boom and Russel, 1993). Probenecid was only a weak inhibitor, with an IC_{50} value (700 μM) greater than the unbound plasma concentration employed in this study. Organic cation transporter(s) will play a major role in the renal uptake of cimetidine, whereas the uptake by the isolated rat CP is totally accounted for by the organic anion transporter. This unique phenomenon is entirely due to the unique nature of the bisubstrate, which is a substrate of both organic anion and cation transporters.

The results of the present study suggest the possibility of drug-drug interactions between the H_2-receptor antagonists and organic anions that cause an increase in the CSF concentration of H_2-receptor antagonists without affecting their plasma concentration profiles, as in the case of probenecid. The risk of mental confusion with cimetidine in patients with renal or hepatic dysfunction is higher than that in normal patients (Schentag et al., 1981). Furthermore, Schentag et al. (1979) reported that the concentration of cimetidine in the CSF is related to the mental status. The $C_{CSF}/C_{p,fu}$ ratio in patients with hepatic dysfunction was 2-fold greater than normal patients, whereas the plasma clearance by both types of patients was not significantly different (Schentag et al., 1979, 1981). These phenomena might be attributed to the inhibition of the efflux transport across the CP by endogenous compounds accumulated in the body due to hepatic dysfunction. Indeed, some organic anions (e.g., quinolinic acid) are known to be elevated in the CSF of patients with hepatic dysfunction (Moroni et al., 1986).

In conclusion, cimetidine and ranitidine are good substrates for rOat3, whereas famotidine is a poor substrate for this transporter. The efflux transport across the CP plays an important role in regulating the CSF concentration of H_2-receptor antagonists. rOat3 is the most likely candidate transporter for the uptake of H_2-receptor antagonists by the isolated rat CP.

References

Boom SP and Russel FG (1993) Cimetidine uptake and interactions with cationic drugs in freshly isolated proximal tubular cells of the rat. *J Pharmacol Exp Ther* **267**:1039–1044.

Burckhardt BC and Burckhardt G (2003) Transport of organic anions across the basolateral membrane of proximal tubule cells. *Rev Physiol Biochem Pharmacol* **146**:95–158.

Choudhuri S, Cherrington NJ, Li N, and Klaassen CD (2003) Constitutive expression of various xenobiotic and endobiotic transporter mRNAs in the choroid plexus of rats. *Drug Metab Dispos* **31**:1337–1345.

Danielle WH and Wright SH (2003) The molecular and cellular physiology of basolateral organic anion transport in mammalian renal tubules. *Biochim Biophys Acta* **1618**:185–193.

Ghersi-Egea JF and Strazielle N (2001) Brain drug delivery, drug metabolism and multidrug resistance at the choroid plexus. *Microsc Res Tech* **52**:83–88.

Grimson T (1977) Reactions to cimetidine. *Lancet* **1**:858.

Grundemann D, Liebich G, Kiefer N, Koster S, and Schomig E (1999) Selective substrates for non-neuronal monoamine transporters. *Mol Pharmacol* **56**:1–10.

Hasegawa M, Kusuhara H, Endou H, and Sugiyama Y (2003) Contribution of organic anion transporters to the renal uptake of anionic compounds and nucleoside derivatives in rat. *J Pharmacol Exp Ther* **305**:1087–1097.

Hasegawa M, Kusuhara H, Sugiyama D, Ito K, Ueda S, Endou H, and Sugiyama Y (2002) Functional involvement of rat organic anion transporter 3 (rOat3; Slc22a8) in the renal uptake of organic anions. *J Pharmacol Exp Ther* **300**:746–753.

Haselbach M, Wegener J, Decker S, Engelbertz C, and Galla HJ (2001) Porcine choroid plexus epithelial cells in culture: regulation of barrier properties and transport processes. *Microsc Res Tech* **52**:137–152.

Kusuhara H, Sekine T, Utsunomiya-Tate N, Tsuda M, Kojima R, Cha SH, Sugiyama Y, Kanai Y, and Endou H (1999) Molecular cloning and characterization of a new multispecific organic anion transporter from rat brain. *J Biol Chem* **274**:13675–13680.

Kusuhara H and Sugiyama Y (2001) Efflux transport systems for drugs at the blood-brain barrier and blood-cerebrospinal fluid barrier (Part 1). *Drug Discov Today* **6**:150–156.

McGuigan J (1981) A consideration of the adverse effects of cimetidine. *Gastroenterology* **80**:181–192.

Moroni F, Lombardi G, Carla V, Lal S, Etienne P, and Nair N (1986) Increase in the content of quinolinic acid in cerebrospinal fluid and frontal cortex of patients with hepatic failure. *J Neurochem* **47**:1667–1671.

Nagata Y, Kusuhara H, Endou H, and Sugiyama Y (2002) Expression and functional characterization of rat organic anion transporter 3 (rOat3) in the choroid plexus. *Mol Pharmacol* **61**:982–988.

Schentag JJ, Cerra FB, Calleri G, DeGlopper E, Rose JQ, and Bernhard H (1979) Pharmacokinetic and clinical studies in patients with cimetidine-associated mental confusion. *Lancet* **1**:177–181.

Schentag JJ, Cerra FB, Calleri GM, Leising MF, French MA, and Bernhard H (1981) Age,

disease and cimetidine disposition in healthy subjects and chronically ill patients. *Clin Pharmacol Ther* 29:737–743.

Segal MB (2000) The choroid plexuses and the barriers between the blood and the cerebrospinal fluid. *Cell Mol Neurobiol* 20:183–196.

Strazielle N, Belin MF, and Ghersi-Egea JF (2003) Choroid plexus controls brain availability of anti-HIV nucleoside analogs via pharmacologically inhibitable organic anion transporters. *AIDS* 17:1473–1485.

Sugiyama D, Kusuhara H, Shitara Y, Abe T, Meier PJ, Sekine T, Endou H, Suzuki H, and Sugiyama Y (2001) Characterization of the efflux transport of 17beta-estradiol-D-17beta-glucuronide from the brain across the blood-brain barrier. *J Pharmacol Exp Ther* 298:316–322.

Suzuki H, Sawada Y, Sugiyama Y, Iga T, and Hanano M (1985) Saturable transport of cimetidine from cerebrospinal fluid to blood in rats. *J Pharmacobio-Dyn* 8:73–76.

Suzuki H, Sawada Y, Sugiyama Y, Iga T, and Hanano M (1986) Transport of cimetidine by the rat choroid plexus in vitro. *J Pharmacol Exp Ther* 239:927–935.

Suzuki H, Sawada Y, Sugiyama Y, Iga T, and Hanano M (1987) Transport of benzylpenicillin by the rat choroid plexus in vitro. *J Pharmacol Exp Ther* 242:660–665.

Suzuki H, Sawada Y, Sugiyama Y, Iga T, and Hanano M (1988) Efflux of cimetidine from the rat cerebrospinal fluid. *Drug Metab Dispos* 16:328–330.

Suzuki H, Terasaki T, and Sugiyama Y (1997) Role of efflux transport across the blood-brain barrier and blood cerebrospinal fluid barrier on the disposition of xenobiotics in the central nervous system. *Adv Drug Delivery Rev* 25:257–285.

Sweet DH, Miller DS, and Pritchard JB (2001) Ventricular choline transport: a role for organic cation transporter 2 expressed in choroid plexus. *J Biol Chem* 276:41611–41619.

Sweet DH, Miller DS, Pritchard JB, Fujiwara Y, Beier DR, and Nigam SK (2002) Impaired organic anion transport in kidney and choroid plexus of organic anion transporter 3 (Oat3 (Slc22a8)) knockout mice. *J Biol Chem* 277:26934–26943.

Ullrich KJ, Rumrich G, David C, and Fritzsch G (1993) Bisubstrates: substances that interact with renal contraluminal organic anion and organic cation transport systems. I. Amines, piperidines, piperazines, azepines, pyridines, quinolines, imidazoles, thiazoles, guanidines and hydrazines. *Pflugers Arch* 425:280–299.

Villalobos AR, Parmelee JT, and Pritchard JB (1997) Functional characterization of choroid plexus epithelial cells in primary culture. *J Pharmacol Exp Ther* 282:1109–1116.

Yamaoka K, Tanigawara Y, Nakagawa T, and Uno T (1981) A pharmacokinetic analysis program (multi) for microcomputer. *J Pharmacobio-Dyn* 4:879–885.

Address correspondence to: Dr. Yuichi Sugiyama, Graduate School of Pharmaceutical Sciences, the University of Tokyo, 7-3-1, Hongo, Bunkyo-ku, Tokyo 113-0033, Japan. E-mail: sugiyama@mol.f.u-tokyo.ac.jp

0022-3565/04/3093-1282–1290$20.00
THE JOURNAL OF PHARMACOLOGY AND EXPERIMENTAL THERAPEUTICS
Copyright © 2004 by The American Society for Pharmacology and Experimental Therapeutics
JPET 309:1282–1290, 2004

Vol. 309, No. 3
61671/1152644
Printed in U.S.A.

Isolation and Characterization of a New Major Intestinal CYP3A Form, CYP3A62, in the Rat

T. Matsubara, H. J. Kim, M. Miyata, M. Shimada, K. Nagata, and Y. Yamazoe

Division of Drug Metabolism and Molecular Toxicology, Graduate School of Pharmaceutical Sciences, Tohoku University, Sendai, Japan

Received October 19, 2003; accepted March 4, 2004

ABSTRACT

Based on information of the nucleotide sequence obtained from rat genome clones, a new CYP3A (CYP3A62) cDNA was isolated from the cDNA library of a rat liver. The CYP3A62 cDNA was 1746 base pairs (bp) in length, which included 1491 bp of an open reading frame and 93 bp and 209 bp of the respective 5′- and 3′-noncoding regions. Amino acid sequence deduced from CYP3A62 cDNA shared the highest similarity with rat CYP3A9 (79.9%) among human and rat CYP3A forms previously reported. CYP3A62 mRNA and protein were consistently detected in small intestines as well as livers. CYP3A62 was a major form in small intestines of both sexes but was a female-predominant form in livers of adult rats. CYP3A62 in both tissues of male and female rats were clearly enhanced by the treatment with dexamethasone. These expression profiles resembled those of CYP3A9. Despite clear detection of CYP3A62, no detectable levels of CYP3A1 and CYP3A2 proteins, as well as those of mRNAs, were found in the intestinal tract. Therefore, CYP3A62 may play major roles together with CYP3A9 and CYP3A18 in endogenous or exogenous detoxification at the absorption site.

The CYP3A subfamily consists of several forms that display considerable extents of similarity with one another in their molecular weights, immunochemical properties, and substrate specificities (Gonzalez, 1988; Nelson et al., 1996). Human CYP3A forms metabolize more than about half of therapeutic drugs (Cholerton et al., 1992; Li et al., 1995) and are also involved in the metabolism of endogenous chemicals such as bile acids (Araya and Wikvall, 1999), steroid hormones (Waxman et al., 1988), and retinoic acid (Marill et al., 2000). CYP3A forms are expressed predominantly in the liver but are also found in other organs such as the gut (Kolars et al., 1994), white blood cells (Janardan et al., 1996; Sempoux et al., 1999), and brain (Wang et al., 1996). The level of CYP3A4 in the intestine is reported to share more than 50% of the total cytochrome P450 (P450) content (Zhang et al., 1999).

In rats, CYP3A1 (Gonzalez et al., 1985), CYP3A2 (Gonzalez et al., 1986), CYP3A9 (Wang et al., 1996), CYP3A18 (Strotkamp et al., 1995; Nagata et al., 1996), and CYP3A23 (Kirita and Matsubara, 1993; Komori and Oda, 1994) have been reported as rat CYP3A forms. CYP3A23 was, however, identified to be the same form as CYP3A1 by analysis of the *CYP3A1* gene (Nagata et al., 1999). These CYP3A forms appear in a sex-dependent manner in rats. For example, CYP3A2 (Yamazoe et al., 1988; Cooper et al., 1993) and CYP3A18 (Nagata et al., 1996; Robertson et al., 1998) are male-specific forms, whereas CYP3A9 is a female-dominant form (Wang and Strobel, 1997; Robertson et al., 1998). The expression profiles in the intestinal tract, however, are obscure with all of the forms.

Levels of CYP3A forms are enhanced after treatment with structurally diverse compounds such as dexamethasone, clotrimazole, and rifampicin (Hostetler et al., 1989; Daujat et al., 1991; Burger et al., 1992; Kocarek et al., 1995). Intestinal CYP3A forms play important roles on the first-pass effect of drugs. In humans, however, rather distinct controls of hepatic and small intestinal CYP3A4s were suggested from experiments using CYP3A4 probe drugs and also from the protein levels. Thus, an understanding of their enzymatic and molecular biological properties is necessary before predicting drug-drug interaction.

As the results of the genome sequencing in various experimental animal species, a number of unidentified genes have been found to provide the information of a novel protein. We have previously isolated six different *CYP3A*-related DNA clones from a rat genomic library (K. Nagata, T. Matsubara, and Y. Yamazoe, unpublished data). The four DNA clones contained information on a part of the first exon boundary of

Article, publication date, and citation information can be found at http://jpet.aspetjournals.org.
DOI: 10.1124/jpet.103.061671.

ABBREVIATIONS: P450, cytochrome P450; PCR, polymerase chain reaction; PAGE, polyacrylamide gel electrophoresis; G6PDH, glucose-6-phosphate dehydrogenase; RT-PCR, reverse transcription-polymerase chain reaction; bp, base pair; HNF-4α, hepatocyte nuclear factor-4α.

CYP3A1, *CYP3A2*, *CYP3A9*, and *CYP3A18* genes, whereas the other two remained unidentified.

In the present study, we have isolated a novel CYP3A cDNA encoding CYP3A62 from rat liver cDNAs. We have also characterized enzymatic and molecular biological properties of this new form in comparison with the other four rat CYP3A forms.

Materials and Methods

Materials. Restriction endonucleases and enzymes were purchased from Takara (Kyoto, Japan). Alkaline phosphatase-conjugated goat anti-rabbit IgG was purchased from Sigma-Aldrich (St. Louis, MO). A mammalian expression vector, pCMV4, was provided by Dr. David W. Russell (University of Texas Southwestern Medical Center, Dallas, TX). Dulbecco's modified Eagle's medium and fetal calf serum were obtained from Invitrogen (Carlsbad, CA), and other chemicals were obtained from Sigma-Aldrich and Wako Pure Chemicals (Osaka, Japan).

Isolation and Sequencing of CYP3A62 cDNA. Oligonucleotide primers used for isolation of CYP3A62 cDNA were 5′-GCAGCACACACAAGCTAAGAA-3′ (fragment 1), 5′-CTGTGACCTATGATGTCCTG-3′ (fragment 2), and 5′-AGCAGCAATGGACCTGATCC-3′ (fragment 3) for the forward primers, and 5′-GAGAGCAAACCTCATGCC-3′ (fragment 1), 5′-TTTTTTTTTTTTTTTTTTT-3′ (fragment 2), and 5′-CCACTCATGGTTCAATC-3′ (fragment 3) for the reverse primers, respectively. DNA fragments from the liver cDNAs of a male adult rat were amplified by the use of Takara *Taq* (Takara, Kyoto, Japan). The reaction mixture (30 μl) contained 1 μl of the template DNA solution, 20 pmol of each of the forward and reverse primers, 250 μM dATP, dCTP, dTTP, and dGTP each, and 1 unit of *Taq* polymerase. After initial denaturation at 94°C for 5 min, the amplification was carried out for 30 cycles with 0.5 min at 94°C for denaturation, 1 min at 55°C for annealing, 1.5 min at 72°C for extension, and a final extension period of 7 min at 72°C.

Transfection of CYP3As into COS-1 Cells and Expression of CYP3A Forms. Constructions of plasmids for CYP3A62, CYP3A9, and CYP3A18 cDNAs were carried out by insertion between the *Mlu*I and *Bgl*II sites of pCMV4; constructions of plasmids for CYP3A1 and CYP3A2 cDNAs were carried out by insertion into the *Eco*RI sites of p91023(B) as reported previously under *Methods* (Miyata et al., 1994; Nagata et al., 1999). These cDNAs were isolated from rat male DNA libraries using a PCR method. These plasmid constructs (50 μg) were transfected into COS-1 cells (2.0×10^6 cells) using an electroporation method. The COS-1 cells cultured at 37°C for 72 h were collected in 2 ml of phosphate-buffered saline. The precipitated cells were resuspended in 100 μl of 75 mM potassium phosphate buffer (pH 7.4) after centrifugation at 2000*g* for 5 min and then homogenized. The homogenate was centrifuged at 9000*g* for 20 min. The supernatant was further centrifuged at 105,000*g* for 60 min, and the microsomal pellet was resuspended in 50 μl of buffer (20% glycerol in 0.1 M potassium phosphate buffer; pH 7.4). Cytochrome P450 content was estimated by the method of Omura and Sato (1964).

Treatment of Animals and Preparation of Microsomes. Male and female Sprague-Dawley rats (10 weeks old) purchased from Japan SLC (Shizuoka, Japan) were acclimated for 3 days. They were divided into three groups (control, dexamethasone-treated, and lithocholic acid-treated). Dexamethasone suspended in corn oil was given intraperitoneally to rats at a dose of 100 mg/kg/day for 3 consecutive days. Lithocholic acid was given orally at a dose of 100 mg/kg/day for 3 consecutive days. Corn oil (1 ml/head) was given to the controls. Microsomes and total RNAs were prepared 20 h after the last dose. Microsomes were prepared as previously described (Yamazoe et al., 1986). Intestinal mucosa microsomes were prepared as follows. The small intestine removed was immediately placed in liquid nitrogen. The tissue cut into small pieces was added to ice-cold buffer (75 mM potassium phosphate buffer, pH 7.4, containing 1 mM EDTA, 1 mM phenylmethylsulfonyl fluoride, 100 μg/ml trypsin inhibitor, and 19 μg/ml aprotinin). The microsomal fraction was isolated using the procedure described for liver microsomes. Microsomal protein was determined by the method of Lowry et al. (1951).

Immunoblot Analysis. Microsomal proteins were electrophoresed in 16 cm of a 7.5% SDS-PAGE for separation and 1 cm of a 2.0% SDS-PAGE for stacking and transferred to a nitrocellulose membrane. The sheet was immunostained with human anti-CYP3A antibody prepared as described previously (Kawano et al., 1987), alkaline phosphatase-conjugated goat anti-rabbit IgG, 5-bromo-4-chloro-3-indolylphosphate, and nitro blue tetrazonium as described previously (Blake et al., 1984).

Testosterone Hydroxylation. The reaction mixture for measurement of testosterone 6β-hydroxylase activities consists of 50 μg of protein of COS-1 microsomes expressing a CYP3A form, 100 mM potassium phosphate buffer (pH 7.4), 5 pmol of cytochrome b_5, 0.1 unit (0.1 mmol of cytochrome *c* per minute) of NADPH-P450 reductase, and 5 μg of sodium cholate in a final volume of 100 μl. The reaction was started by the addition of NADPH (final concentration, 0.5 mM) and terminated by adding ethyl acetate after 40 min of incubation at 37°C. Testosterone hydroxylation was quantified by the method described previously (Yamazoe et al., 1988; Guo et al., 2000).

Amiodarone and Lidocaine De-ethylations. The reaction mixtures for amiodarone and lidocaine *N*-de-ethylase activities consisted of 50 μg of protein of COS-1 microsomes expressing a CYP3A form, 100 mM potassium phosphate buffer (pH 7.4), 5 pmol of cytochrome b_5, 0.1 unit of NADPH-P450 reductase, 5 μg of sodium cholate, and 200 nmol of amiodarone or lidocaine in a final volume of 100 μl. The reaction was started by the addition of NADPH (final concentration, 0.5 mM) and then terminated by the addition of zinc sulfate and barium hydroxide after 40 min of incubation at 37°C. The acetaldehyde thus formed was converted to a decahydroacridine derivative using the reaction with 4 μg of 1,3-cyclohexandione, 4 mg of ammonium acetate, and 2 mg of acetic acid at 80°C for 30 min in a final volume of 300 μl. The derived product was quantified using a high-performance liquid chromatography system equipped with a C_{18} reversed-phase analytical column (particle size, 7 μm, 4.6 × 150 mm). The metabolites were detected with the fluorescence at excitation and fluorescence wavelengths of 390 and 457 nm, respectively. The sample was eluted using acetonitrile/0.5% acetic acid in distilled water (1:4) at a flow rate of 1 ml/min.

Analysis of Rat CYP3A mRNAs. Total RNA was extracted from the following tissues: liver, kidney, spleen, lung, heart, adrenal, brain, stomach, duodenum, jejunum, ileum, colon, testis, prostate, ovary, and uterus of male and female rats using an acid guanidinium

TABLE 1
Primer used in PCR reaction for mRNA detection and quantification

Messenger	Forward Primer	Reverse Primer	Fragment Size
CYP3A62	5′-GGAGATAAAGAGTCTCACC-3′	5′-AGTTCTGCAGGACTCAGAC-3′	544
CYP3A1	5′-GGAGATCACAGCCCAGTCAATC-3′	5′-TGGCCAGTGCTGTGGATCAC-3′	349
CYP3A2	5′-CAAGGGAGATGTTCCCCATCATTG-3′	5′-GCTATGATTTCAACATCAGAC-3′	469
CYP3A9	5′-CCATAACATCAATCCTTATATG-3′	5′-GCACGCGTGATACAACACCACTATAGGC-3′	276
CYP3A18	5′-CCAATCTATCCTCTTCATCGGA-3′	5′-CCCCGGGAAATTCACTGTCC-3′	326
G6PDH	5′-GAAGCAGTCACCAAGAAC-3′	5′-CTGCATGACATCCCTGATGATC-3′	332

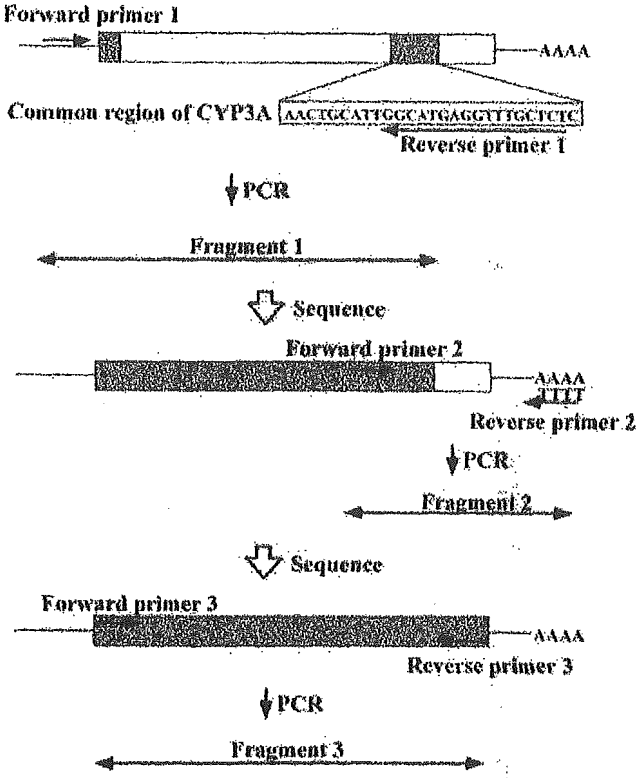

Fig. 1. The strategy for isolation of CYP3A62 cDNA. Boxes represent the cording region. Identified or predicted regions are shown as hatched.

thiocyanate-phenol-chloroform method. Total RNAs of each tissue were combined for a pool of four individuals. The cDNA was reverse-transcripted from those total RNAs with Ready-To-Go (Amersham Biosciences Inc., Piscataway, NJ). The nucleotide sequences of CYP3A62-, CYP3A1-, CYP3A2-, CYP3A9-, CYP3A18-, and G6PDH-selective oligonucleotide primers are shown in Table 1. cDNA fragments for CYP3A62, CYP3A1, CYP3A2, CYP3A9, CYP3A18, and G6PDH were amplified by use of Takara *Taq*. The reaction mixture (30 μl) contained 1 μl of the cDNA solution as a template DNA, 20 pmol of each forward and reverse primer as described above, 250 μM dATP, dCTP, dTTP, and dGTP each, 1 unit each of the enzyme and the buffer. After initial denaturation at 94°C for 5 min, the targeted nucleotides were amplified for 35 cycles (RT-PCR) or 40 cycles (real-time PCR), with 30 s at 94°C for denaturation, 15 s at 55°C (CYP3A9 and G6PDH), 60°C (CYP3A62 and CYP3A2), or 63°C (CYP3A1 and CYP3A18) for annealing, 30 s at 72°C for extension, and a final extension period of 7 min at 72°C. The quantification of mRNAs was carried out with SYBR Green by using ABI PRISM 7000 (Applied Biosystems, Foster City, CA). A real-time PCR method was used to determine the expression amounts of CYP3A mRNAs in various rat tissues. In these experiments, levels of CYP3A mRNAs were normalized from the amount of total RNA.

Results

Isolation and Analysis of CYP3A62 cDNA. In previous experiments, we have identified six different promoter regions of CYP3A genes from rats. Four of them were matched to genes encoding the first exon regions of CYP3A forms [(*CYP3A1* (Gonzalez et al., 1985), *CYP3A2* (Gonzalez et al., 1986), *CYP3A9* (Wang et al., 1996), and *CYP3A18* (Nagata et al., 1996), respectively] that were identified previously. The other two clones seemed to encode unknown CYP3A genes. Based on this information, a novel CYP3A form (CYP3A62) cDNA has been isolated using RT-PCR. A fragment 1 of CYP3A62 cDNA was at first amplified from the liver cDNA of a male adult rat with the forward primer 1 and reverse primer 1 (Fig. 1), and the nucleotide sequence was deter-

TABLE 2

Homology of amino acid sequence among CYP3A forms. CYP3A1, K. Nagata (L24207); CYP3A2, M. Miyata (NM_153312); CYP3A9, P. Nef (NM_147206); CYP3A18, K. Nagata (NM_145782); CYP3A4, T. Molowa (NM_017460); CYP3A5, T. Aoyama (NM_000777); CYP3A7, M. Komori (NM_000765); CYP3A43, T. L. Domonski (AF319634).

	CYP3A1	CYP3A2	CYP3A9	CYP3A18	CYP3A4	CYP3A5	CYP3A7	CYP3A43
CYP3A62	69.3	67.7	79.9	67.2	71.6	73.4	69.8	67.0
CYP3A1		86.3	72.6	69.7	71.8	71.6	68.8	63.1
CYP3A2			72.2	67.1	72.0	70.8	69.2	63.5
CYP3A9				68.4	76.5	75.1	72.8	68.0
CYP3A18					68.4	68.6	65.2	64.4
CYP3A4						84.3	88.3	75.7
CYP3A5							81.9	75.7
CYP3A7								71.4

TABLE 3

The quantification of male and female rat CYP3A mRNAs by real-time PCR in liver and intestinal tract. Real-time PCR was carried out as described under *Materials and Methods*. The numbers represent the molecular number of CYP3A mRNA to total RNA amount (attomole of CYP3A mRNA/μg total RNA). The limit of detectable CYP3A mRNAs was less than 0.01 attomoles of CYP3A mRNA/μg of total RNA.

Sex	Tissue	Cytochrome P450				
		CYP3A62	CYP3A1	CYP3A2	CYP3A9	CYP3A18
Male	Liver	1.05	52.48	382.69	3.97	6.29
	Duodenum	9.61	N.D.	N.D.	12.42	0.39
	Jejunum	7.88	N.D.	N.D.	8.49	0.55
	Ileum	5.50	N.D.	N.D.	1.11	0.25
	Colon	3.01	N.D.	N.D.	0.89	0.04
Female	Liver	5.73	39.09	N.D.	12.94	0.97
	Duodenum	7.27	N.D.	N.D.	0.61	0.10
	Jejunum	2.54	N.D.	N.D.	0.11	0.10
	Ileum	1.09	N.D.	N.D.	0.04	0.07
	Colon	0.24	N.D.	N.D.	0.14	N.D.

N.D., not detectable.

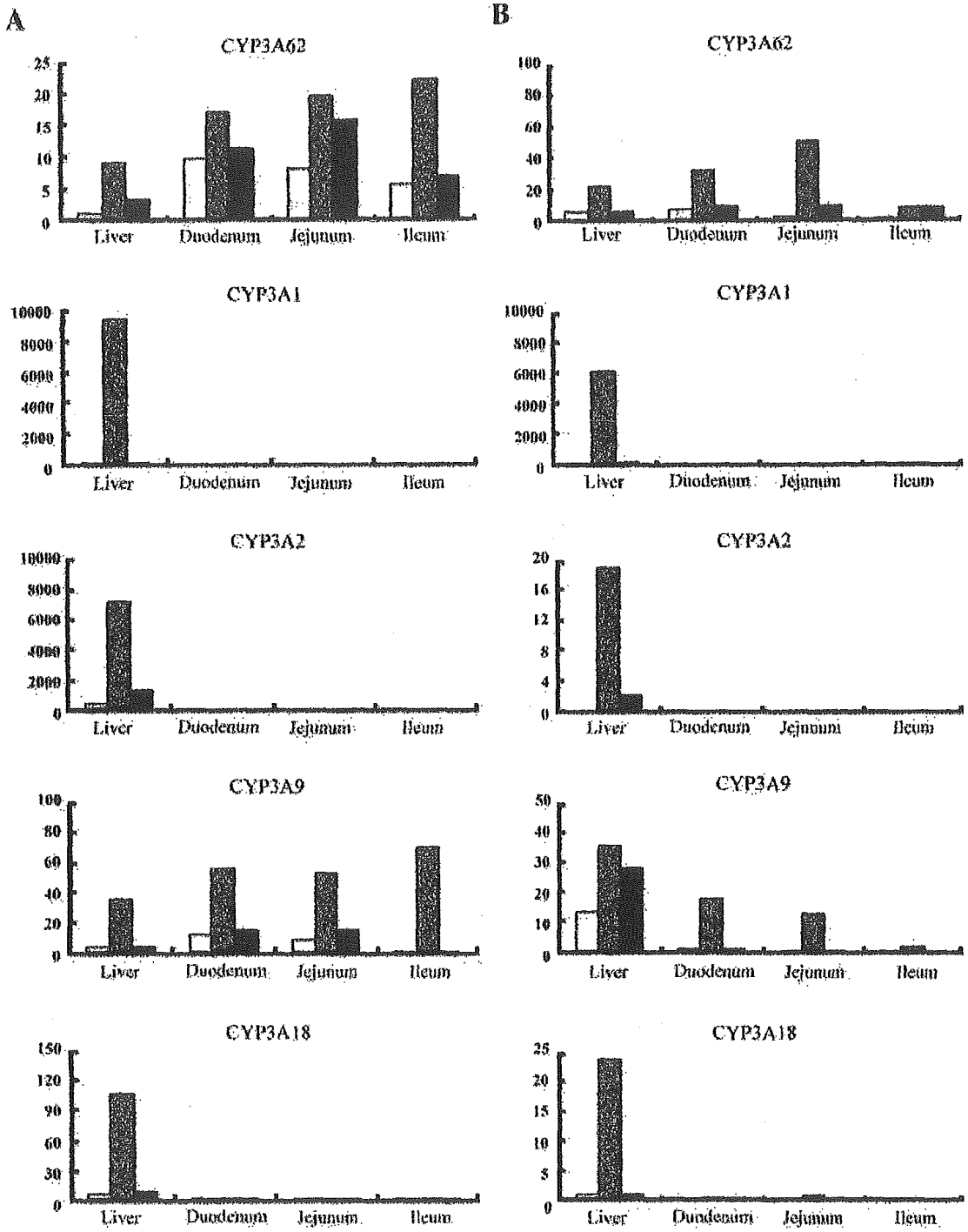

Fig. 2. Changes in the profile of rat CYP3A mRNAs after treatment with dexamethasone or lithocholic acid in liver and intestinal tract. Real-time PCR and drug treatment were carried out as described under *Materials and Methods*. A, male rat; B, female rat. Semiclosed column, closed column, and open column represent the rat group treated with dexamethasone, treated with lithocholic acid, and the control group, respectively. The numbers in this figure represent the molecular number of CYP3A mRNA to total RNA amount (attomole per microgram). The limit of detectable CYP3A mRNAs was less than 0.01 attomoles of CYP3A mRNA/μg total RNA.

mined. The reverse primer 1 was constructed from a region of highly conserved nucleotide sequences among CYP3A cDNAs. Second, a fragment 2 was amplified with the forward primer 2 and reverse primer 2 to determine the nucleotide sequence. Finally, fragment 3 of the CYP3A62 cDNA, including an entire open reading frame, was amplified from the rat liver cDNAs with the forward primer 3 and reverse primer 3. The nucleotide sequence of fragment 3 was completely identical with those of fragments 1 and 2 (Fig. 1). In this strategy, the identified cDNA was 1746 bp in length, which had an open reading frame of 1491 bp (corresponding to 497 amino acids), 93 bp and 209 bp of the 5′- and 3′-noncoding regions,

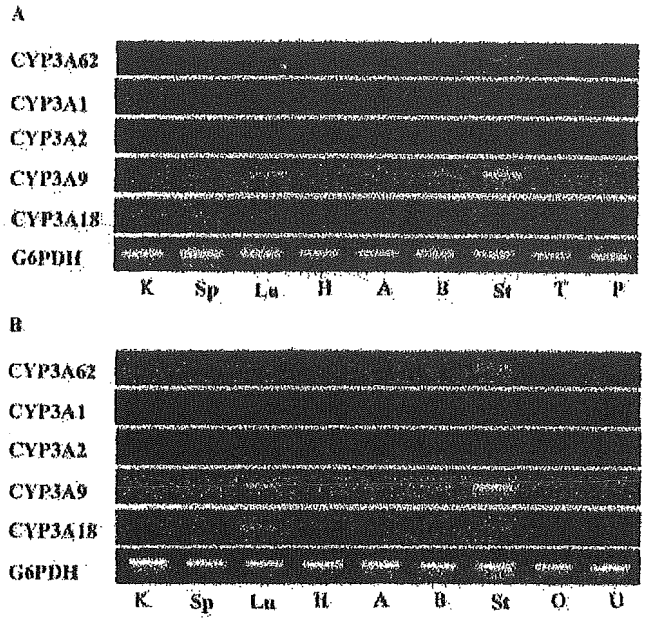

Fig. 3. Detection of rat CYP3A mRNAs in tissues other than liver and intestine. RT-PCR was carried out as described under *Materials and Methods*. Electrophoresis was performed in a 1% agarose gel. A, male rat tissues; B, female rat tissues. Lanes: K, kidney; Sp, spleen; Lu, lung; H, heart; A, adrenal; B, brain; St, stomach; Te, testis; P, prostate; O, ovary; U, uterus.

respectively. This nucleotide sequence was deposited with the DDBJ nucleotide sequence database (Accession no. AB084894). CYP3A62 cDNA showed the highest similarity in the nucleotide sequence with rat CYP3A9 and mouse Cyp3a13 cDNAs (both 84.4%). CYP3A62 showed the highest similarity with CYP3A9 (79.9%) and also showed 67.0 to 73.4% similarity in amino acid sequence with other rat and human CYP3A forms (Table 2). A unique property of this new form is in the number of cording residues. A nucleotide change (change A to T) at 1584 bp of CYP3A62 cDNA to form a termination codon resulted in 3- or 6-amino acid shorter sequences as compared with those of other CYP3A forms except for CYP3A18.

Quantification of CYP3A mRNAs in Liver and Intestinal Tract. The quantification of individual CYP3A mRNAs was carried out by the use of a real-time PCR method. As shown in Table 3, predominant expression of CYP3A62 mRNA and CYP3A9 mRNA in the female over the male was observed in the liver. The level of CYP3A62 mRNA was about 5 times higher in the female than in the male in liver (5.73 and 1.05 attomole/μg total RNA, respectively). CYP3A62 mRNA was also detected in the intestinal tract of both sexes. The level was rather higher in the male intestinal tract than in the liver (duodenum, jejunum, ileum, and colon were 9.61, 7.88, 5.50, and 3.01 attomole/μg total RNA, respectively). In female rats, the level was roughly equivalent between the liver and duodenum (5.73 and 7.27 attomole/μg total RNA, respectively), and lower in the jejunum, ileum, and colon than in the duodenum (jejunum, ileum, and colon were 2.54, 1.09, and 0.24 attomole/μg total RNA, respectively). Their tissue distribution profiles were similar to those of CYP3A9 mRNA. CYP3A2 and CYP3A18 mRNAs were predominantly expressed in male rat livers as previously reported (Cooper et al., 1993; Robertson et al., 1998). The amount of CYP3A2 mRNA was highest among rat CYP3A forms (382.69 attomole/μg total RNA). CYP3A1 mRNA was also observed in livers of both sexes (male and female were 52.48 and 39.09 attomole/μg total RNA, respectively), although the levels were lower than that of CYP3A2 mRNA in male rats. An interesting thing is that CYP3A1 and CYP3A2 mRNAs were

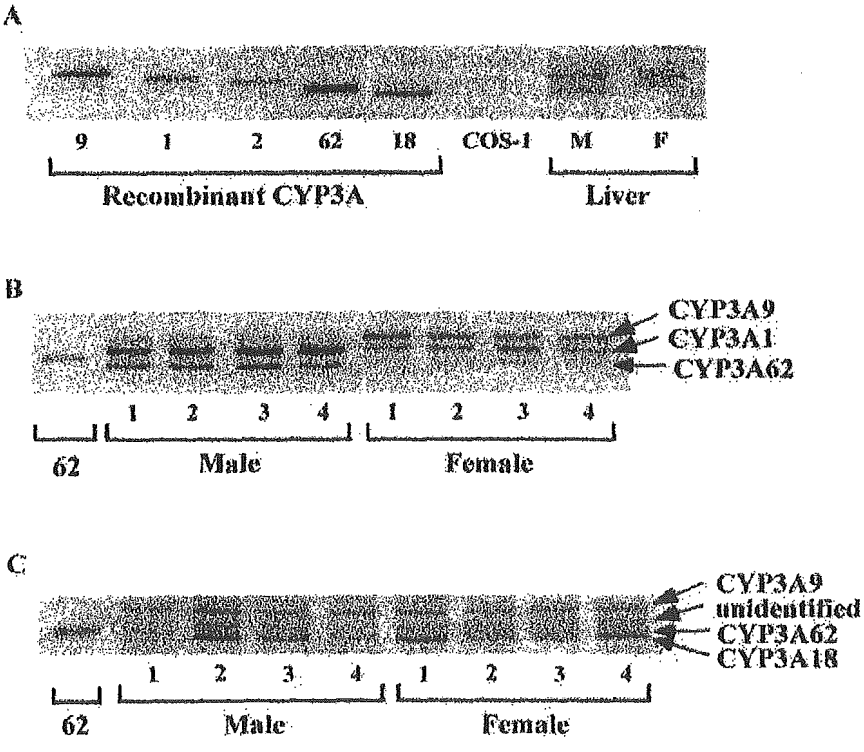

Fig. 4. Western blot analyses of microsomal proteins in rat liver and small intestine. Electrophoresis was performed in a 7.5% SDS-PAGE. The blotted membrane was proved with the anti-CYP3A antibody. Details are described under *Materials and Methods*. A, recombinant CYP3A forms. Lanes: 9, 2 μg of CYP3A9 microsomes; 1, 2 μg of CYP3A1 microsomes; 2, 2 μg of CYP3A2 microsomes; 62, 2 μg of CYP3A62 microsomes; 18, 2 μg of CYP3A18 microsomes; COS-1, 2 μg of COS-1 microsomes; M, 2 μg of microsomes pooled from four male rat livers; F, 2 μg of microsomes pooled from four female rat livers. B, rat liver. Lanes: 62, 4 μg CYP3A62 microsomes; Male, 10 μg male microsomes; Female, 10 μg of female microsomes. C, rat small intestine. Lanes: 62, 6 μg of CYP3A62 microsomes; Male, 50 μg of male microsomes; Female, 50 μg of female microsomes.

not detected in the intestinal tract using real-time PCR. CYP3A18 mRNA was detected as a male-predominant form in the liver and intestinal tract, although the level was very low in the intestinal tract.

After treatment of rats with dexamethasone intraperitoneally, both CYP3A1 and CYP3A2 mRNAs were clearly increased (25 to 200 times) in the liver but not at all in the intestinal tracts as shown in Fig. 2. CYP3A18 mRNA was also enhanced in the liver (about 20 times) and to a lesser extent in the ileum (2–4 times). The expression profile of CYP3A62 mRNA differed from those of CYP3A1, CYP3A2, and CYP3A18 mRNAs. Levels of CYP3A62 mRNA were increased in both liver and intestinal tracts of both sexes (2–30 times) by the treatment. Similar profiles were also detected in the level of CYP3A9 mRNA. These results were confirmed by repeated experiments (data not shown). On the other hand, only CYP3A2 mRNA was strongly increased in the liver of both sexes after treatment with lithocholic acid. In the jejunum of both sexes, CYP3A62 mRNA was increased (2–5 times) by the treatment.

Tissue Distribution of CYP3A62 and Other Rat CYP3A Forms. To assess the tissue distribution of rat CYP3A forms other than liver and intestine, selectively amplified mRNA levels were detected in various tissues by RT-PCR with specific primers as shown in Table 1. The band for CYP3A62 mRNA was found in the stomach of both sexes (Fig. 3). CYP3A9 mRNA was detected in the stomach, lung, and brain of both sexes. CYP3A1 and CYP3A2 mRNAs were also not detected in these tissues. CYP3A18 mRNA was detected in the lungs of both sexes and in the kidney and spleen of the male.

Detection of the CYP3A62 Protein. To characterize the enzymatic properties of a protein derived from CYP3A62 cDNA, all rat CYP3A forms identified were expressed in COS-1 cells as described under *Materials and Methods*. Microsomal proteins in COS-1 cells were immunoblotted by the use of anti-CYP3A antibodies. As shown in Fig. 4A, individual recombinant CYP3A forms expressed in COS-1 cells were clearly separated and detected at different electrophoretic mobilities. The order of those electrophoretic mobilities was CYP3A18, CYP3A62, CYP3A2, CYP3A1, and CYP3A9 from lower dalton registers. The band corresponding to CYP3A62 was detected in the female liver but not clearly in the male liver (Fig. 4B). Bands to CYP3A2 and/or CYP3A1 and CYP3A18 were clearly detected in the male liver, and a band corresponding to CYP3A9 was also detected (Fig. 4B). In livers of female rats, bands of CYP3A1 and CYP3A9 were clearly detected, but not those of CYP3A2 and CYP3A18 (Fig. 4B). In small intestines of both sexes, the bands corresponding to CYP3A62 and CYP3A9 were detected. CYP3A18 was also detected, but the expressed level varied clearly among individuals. An unidentified band was detected in small intestines of both sexes as indicated by the arrow.

Microsomal levels of individual CYP3A forms are summarized in Table 4. Due to overlapping mobilities of CYP3A2 and CYP3A1 in SDS-PAGE, combined amounts are shown for livers of male rats. CYP3A2/CYP3A1 and CYP3A18 had 53.95 and 28.24 pmol/mg protein in male rat livers, respectively. CYP3A9 was 5.12 pmol/mg protein in male rat livers, but CYP3A62 was not clearly quantified (<0.1 pmol/mg protein). On the other hand, CYP3A1 and CYP3A9 had 19.07 and 11.24 pmol/mg protein in female rat livers. CYP3A62 was predominantly detected in female livers (4.81 pmol/mg protein), and CYP3A2 and CYP3A18 in female livers were not detected (<0.1 pmol/mg protein). In small intestines of both sexes, the expressed level of the CYP3A62 was highest among CYP3A forms. The levels of CYP3A62, CYP3A9, and CYP3A18 were quantified at 2.31, 0.78, and 0.84 pmol/mg protein in males, respectively. On the other hand, in females the levels of CYP3A62, CYP3A9, and CYP3A18 were 2.01, 0.73 and 0.89 pmol/mg protein, respectively. Neither CYP3A1 nor CYP3A2 was detected in small intestines of both sexes.

Comparison of Catalytic Activities among Recombinant CYP3A Forms. Testosterone 6β-hydroxylation is known as a typical catalytic activity for CYP3A forms. Some of the members are also known to catalyze 2β- and 15β-hydroxylations of testosterone, although the extent of those activities is lower than that of the 6β-hydroxylation. In the present study, the catalytic property of CYP3A62 was compared with other forms using testosterone hydroxylation. As shown in Table 5B, recombinant CYP3A62 mediated testosterone 6β- and 2β-hydroxylations at the lowest rate (1.14 and 0.06 nmol/min/nmol P450, respectively) among recombinant rat CYP3A forms examined. A catalytic activity of testosterone 16α-hydroxylation (0.76 nmol/min/nmol P450), which could not be detected in CYP3A1, CYP3A2, and CYP3A9, was observed in CYP3A62 as well as in CYP3A18. As shown in Table 5B, CYP3A62 activity was only slightly increased (about 1.3 times) by addition of cytochrome b_5, despite the clear changes in other forms.

To further characterize the drug-metabolizing activity in CYP3A62, catalytic activities of amiodarone and lidocaine *N*-de-ethylations were tested with recombinant rat CYP3A forms. As shown in Table 6, CYP3A62 showed low but clear *N*-de-ethylating activities of both amiodarone and lidocaine (0.007 and 0.054 nmol/min/nmol P450, respectively). In addition, CYP3A9 showed the highest activity of both *N*-de-

TABLE 4

The quantification of CYP3A forms in liver and small intestine of male and female rats. Immunoblot analysis was carried out as described under *Materials and Methods*. The numbers represent the ratio of CYP3A form to microsomal protein (pmol/mg protein). The value represents the mean and the standard deviation of four different rats. <0.10, less than 0.10 pmol/mg protein in liver, and <0.02, less than 0.02 pmol/mg protein in small intestine. The value of CYP3A1 and CYP3A2 forms in male liver represents the total amount of both CYP3A1 and CYP3A2 due to incomplete separation. *, CYP3A62 and CYP3A18 forms were separated incompletely in SDS-PAGE, but the stained band could be divided into two upper (CYP3A62) and lower (CYP3A18) portions by using NIH image 1.59/ppc.

Sex	Tissue	Cytochrome P450				
		CYP3A62	CYP3A1	CYP3A2	CYP3A9	CYP3A18
Male	Liver	<0.10	53.95 ± 4.42		5.12 ± 1.44	28.24 ± 2.29
	Small intestine	2.31 ± 1.33*	<0.02	<0.02	0.78 ± 0.20	0.84 ± 0.82*
Female	Liver	4.81 ± 0.57	11.24 ± 3.29	<0.10	19.07 ± 3.31	<0.10
	Small intestine	2.01 ± 0.33*	<0.02	<0.02	0.73 ± 0.18	0.89 ± 0.50*

TABLE 5

Testosterone hydroxylation by rat recombinant CYP3A forms. The enzyme activity was measured using 50 μg of microsomal protein of COS-1 cells described in detail under *Materials and Methods*. Activities represented are the mean and the standard deviation of three different experiments by nmol/min/nmol P450. 6β-OH, 16α-OH, 2β-OH, and 15β-OH represent the rate of testosterone 6β-, 16α-, 2β-, and 15β-hydroxylase activities, respectively. Cytochrome b_5 (−), without addition of cytochrome b_5; cytochrome b_5 (+), with addition of cytochrome b_5.

A

P450	Testosterone Hydroxylation-Cytochrome b_5 (−)			
	6β-OH	16α-OH	2β-OH	15β-OH
CYP3A62	0.86 ± 0.09	0.61 ± 0.08	0.06 ± 0.00	N.D.
CYP3A1	0.41 ± 0.16	N.D.	0.17 ± 0.01	N.D.
CYP3A2	1.19 ± 0.19	N.D.	0.16 ± 0.01	N.D.
CYP3A9	0.79 ± 0.06	N.D.	0.12 ± 0.00	N.D.
CYP3A18	1.21 ± 0.15	0.44 ± 0.05	0.06 ± 0.00	0.15 ± 0.01

B

P450	Testosterone Hydroxylation-Cytochrome b_5 (+)			
	6β-OH	16α-OH	2β-OH	15β-OH
CYP3A62	1.14 ± 0.16	0.76 ± 0.04	0.06 ± 0.00	N.D.
CYP3A1	2.21 ± 0.19	N.D.	0.48 ± 0.01	N.D.
CYP3A2	10.13 ± 0.91	N.D.	0.46 ± 0.03	N.D.
CYP3A9	2.65 ± 0.19	N.D.	0.19 ± 0.00	N.D.
CYP3A18	3.43 ± 0.56	0.79 ± 0.18	0.12 ± 0.02	0.41 ± 0.06

N.D., not detectable (< 0.02 nmol/min/nmol P450).

TABLE 6

N-De-ethylating activities by rat recombinant CYP3A forms. The enzyme activity was measured using 50 μg of microsomal protein of COS-1 cells described in detail under *Materials and Methods*. Activities represented are the mean and the standard deviation of three different experiments by nmol/min/nmol P450.

P450	Substrate	
	Amiodarone	Lidocaine
CYP3A62	0.008 ± 0.008	0.054 ± 0.012
CYP3A1	0.038 ± 0.005	0.081 ± 0.004
CYP3A2	0.018 ± 0.015	0.174 ± 0.006
CYP3A9	0.156 ± 0.010	0.178 ± 0.007
CYP3A18	0.084 ± 0.008	0.067 ± 0.006

ethylations among rat CYP3A forms (0.156 and 0.178 nmol/min/nmol P450).

Discussion

In our previous experiments with *CYP3A* gene structures, six different *CYP3A* genomic clones were isolated. Four of them were identified to encode exon 1 of the *CYP3A1*, *CYP3A2*, *CYP3A9*, and *CYP3A18* genes, whereas the other two remained unidentified. Based on high similarities of their partial nucleotide sequences and the possible first exon information, a novel rat CYP3A cDNA, CYP3A62 cDNA, has been isolated from a liver cDNA library of a male rat. The entire sequence of the isolated cDNA has 1746 bp and includes an open reading frame of 1491 bp encoding a protein of 497 amino acids. The amino acid number is six residues shorter than those of CYP3A2 and CYP3A9, but it is identical with that of CYP3A18. CYP3A62 showed the highest similarity with CYP3A9 among rat CYP3As and was more similar to human CYP3A4 and CYP3A5 than rat CYP3A1 and CYP3A2 in their amino acid sequences.

CYP3A62 mRNA and CYP3A9 mRNA were detected in the liver and intestinal tract using real-time PCR, and their profiles were similar to one another (Table 3). These profiles were also supported by the quantification of both proteins detected by immunoblot analyses (Fig. 4; Table 4). Another form, CYP3A18, was also detected, but major hepatic forms, CYP3A1 and CYP3A2, were not detected in the intestinal tracts of both sexes (Table 3). This may be related to the difference of catabolic and metabolic activities between livers and small intestines in rats. A large individual variation was observed on the expression level of CYP3A18 protein in the small intestine. The extent of transcriptional activation after the treatment with dexamethasone or lithocholic acid also differs among rat *CYP3A* genes. As shown in Fig. 2, all the CYP3A mRNAs in livers were increased after the treatment of both sexes of rats with dexamethasone. CYP3A1 and CYP3A2 mRNAs were not detected even with real-time PCR in intestines of rats treated with dexamethasone. In contrast, CYP3A62 and CYP3A9 mRNAs were readily detectable and enhanced after dexamethasone treatment in the small intestine and liver. These results clearly indicate the liver-selective expression of CYP3A1 and CYP3A2 and the intestinal-dominant expression of CYP3A62 and CYP3A9. Human CYP3A4 was detected mainly in the liver and intestinal tract and also increased in both tissues after treatment with chemical inducers (Kolars et al., 1992; Goodwin et al., 1999; Schmiedlin-Ren et al., 2001). These expression profiles are more similar to those of CYP3A62 and CYP3A9 than to those of CYP3A1 and CYP3A2. In addition to the expression profile, the nucleotide sequence of the *CYP3A62* proximal promoter region shows higher similarity with that of the *CYP3A4* genes than that of *CYP3A1* and *CYP3A2* genes (Fig. 5). It has been reported that *CYP3A1* and *CYP3A2* genes have hepatocyte nuclear factor-4α (HNF-4α) binding element in their proximal promoter regions (Miyata et al., 1995; Nagata et al., 1999) as shown in Fig. 5. On the other hand, CYP3A62 as well as CYP3A4 do not contain HNF-4α binding element in their proximal promoter regions. Localization of HNF-4α binding site at the proximal promoter region may be associated with the strict liver-specific expression of CYP3A1 and CYP3A2.

Recombinant CYP3A62 mediated testosterone 6β-hydroxylation, but the rate was the lowest among recombinant rat CYP3A forms examined. Microsomal testosterone 6β-hydroxylation of CYP3A62 was slightly enhanced after addition of cytochrome b_5, unlike CYP3A1 and CYP3A2. A profile similar to CYP3A62 on testosterone hydroxylation was observed in that of CYP3A18. As reported, requirement of cytochrome b_5 was dependent on the combination of P450 and substrate (Guengerich, 1983; Schenkman and Jansson, 2003). It may imply that the energy to transfer a second electron from cytochrome b_5 to P450 is different among P450 and/or substrate, but no clear evidence can be provided.

In conclusion, we have isolated a new rat CYP3A form and identified it as CYP3A62 in the present study. Nucleotide sequences of the promoter region and CYP3A62 cDNA exhibited high similarity with the nucleotide sequences of CYP3A4 and CYP3A9 compared with the nucleotide sequences of CYP3A1 and CYP3A2. CYP3A62 was a predominant form in the intestinal tract, whereas CYP3A1 and CYP3A2 were detected only in the liver. In addition, the expression profile of CYP3A62 was also similar to that of CYP3A4 and CYP3A9. Judging from the absence of CYP3A1 and CYP3A2 in the gastrointestinal tract, CYP3A62, as well as CYP3A9 and

```
CYP3A62   ---------- ----TCCTTG ATA-TTTATA CCAAATG-AA TCCAAA----   -173
CYP3A4    ---------- ---GTTTATG ATACCTCATA GAATATG-AA CTCAAA--G-   -159
CYP3A9    CACTGGCCCC TTTTTACTCA ATGTTTCTTA CCAAATG-AA TTCAGA--G-   -162
CYP3A1    ---------- ---------- -TGTTGTTCA CT-GACGCCA CCCAGAATGT   -174
CYP3A2    ---------- ---------A CTGCTGTTTA CT-GATGCCA CACAGAATGT   -172
CYP3A18   ---------- -TACACACAG AAA-TATAAG CT-CAAG--- ----G---G-   -174

CYP3A62   TATCACAGTG ---GGCACAT CCATGATTCT CTGCAAGCTG C-TGAGGTGG   -127
CYP3A4    GAGGTCAGTG AGTGGTGTGT GTGTGATTCT TTGGCAACTT C-CAAGGTGG   -110
CYP3A9    -ATCAAAGTG ---GGTACGT CCATGATCCT TTGCCAACTG C-TAGGTTAG   -116
CYP3A1    TAACTCAAAG -GAGGTCAAA ATA-GGCTGT AGATGAACTT CATGAACTGT   -126
CYP3A2    TAGCTCAA-G A-AGGTCAAA GAA--GCTGT AGATGAACTT TATGAACTGT   -126
CYP3A18   AGGGTCAGAG T-AGGAAAAT GCATGAACTT TTTGGCACTT TGACAAATG-   -126

CYP3A62   AGAAGGCACT GAACTCTTGG A--AC-TGT- AGGT-TTGCC CTGGTAGTGT    -82
CYP3A4    AGAAG---C- ---CTCTTCC A--AC-TGC- AGGCAGAGCA CAGGTGGCCC    -71
CYP3A9    AGAGTACACT TGACTC--AG A--AC-TGT- AGGT-GTTTC CA-TTGG---    -77
CYP3A1    CTAGGGGAAG AGAGT[redacted]GGCAG---- -AGGTGATCC    -81
CYP3A2    TTAGGGGAAG AGAGT[redacted]GCCAG---- -AGGTGATCC    -81
CYP3A18   CCAGGTAGAG GCCACACCAG AACTTCAAGT TCAGGCAATG TGCAAATACC    -76

CYP3A62   TTCTACTAAA CGTAAAACCA GCCCCACCCC CTTTTCCAGT ATTTAAGCAC    -32
CYP3A4    TGCTACTGGC TGCAGCTCCA GCCCTGCCTC CTTCTCTAGC ATATAAACAA    -21
CYP3A9    --CTAC-AAG TTCAGCCCCA ------CCTC CTTTCCCTGT TCTTAAGCAC    -36
CYP3A1    ATCTACTGGC TGGATCCCTG GTGCCACCCA TCTTTCCAGC ATATAAGTAC    -31
CYP3A2    ATCTACTGGT TGGATCCCTG GTGCCACCCA TCTTTCCAGC ATATAAGTAC    -31
CYP3A18   TTGTACTGGA TGTGTCCCCG ACACCTCCCC CTTTCCCGGC AAATAAATAG    -26
```

■:HNF-4α binding site □:putative TATA box

Fig. 5. Comparison of nucleotide sequences of *CYP3A* genes. CYP3A62, T. Matsubara (AB107227); CYP3A4, B. J. Goodwin (AF185589); CYP3A9, T. Matsubara (AB107757); CYP3A1, K. Nagata (AB008389); CYP3A2, M. Miyata (AH005338); and CYP3A18, T. Matsubara (AB107758).

CYP3A18, may play an important role in endogenous or exogenous detoxification at absorption in the small intestine.

References

Araya Z and Wikvall K (1999) 6α-Hydroxylation of taurochenodeoxycholic acid and lithocholic acid by CYP3A4 in human liver microsomes. *Biochim Biophys Acta* **1436**:47–54.

Blake MS, Johnston KH, Russell-Jones GJ, and Gotschlich EC (1984) A rapid, sensitive method for detection of alkaline phosphatase-conjugated anti-antibody on Western blots. *Anal Biochem* **136**:175–179.

Burger HJ, Schuetz JD, Schuetz EG, and Guzelian PS (1992) Paradoxical transcriptional activation of rat liver cytochrome P-450 3A1 by dexamethasone and the antiglucocorticoid pregnenolone 16α-carbonitrile: analysis by transient transfection into primary monolayer cultures of adult rat hepatocytes. *Proc Natl Acad Sci USA* **89**:2145–2149.

Cholerton S, Daly AK, and Idle JR (1992) The role of individual human cytochromes P450 in drug metabolism and clinical response. *Trends Pharmacol Sci* **13**:434–439.

Cooper KO, Reik LM, Jayyosi Z, Bandiera S, Kelley M, Ryan DE, Daniel R, McCluskey SA, Levin W, and Thomas PE (1993) Regulation of two members of the steroid-inducible cytochrome P450 subfamily (3A) in rats. *Arch Biochem Biophys* **301**:345–354.

Daujat M, Pichard L, Fabre I, Pineau T, Fabre G, Bonfils C, and Maurel P (1991) Induction protocols for cytochromes P450IIIA in vivo and in primary cultures of animal and human hepatocytes. *Methods Enzymol* **206**:345–353.

Gonzalez FJ (1988) The molecular biology of cytochrome P450s. *Pharmacol Rev* **40**:243–288.

Gonzalez FJ, Nebert DW, Hardwick JP, and Kasper CB (1985) Complete cDNA and protein sequence of a pregnenolone 16α-carbonitrile-induced cytochrome P-450. *J Biol Chem* **260**:7435–7441.

Gonzalez FJ, Song BJ, and Hardwick JP (1986) Pregnenolone 16α-carbonitrile-inducible P-450 gene family: gene conversion and differential regulation. *Mol Cell Biol* **6**:2969–2976.

Goodwin B, Hodgson E, and Liddle C (1999) The orphan human pregnane X receptor mediates the transcriptional activation of CYP3A4 by rifampicin through a distal enhancer module. *Mol Pharmacol* **56**:1329–1339.

Guengerich FP (1983) Oxidation-reduction properties of rat liver cytochromes P-450 and NADPH-cytochrome p-450 reductase related to catalysis in reconstituted systems. *Biochemistry* **22**:2811–2820.

Guo LQ, Taniguchi M, Xiao YQ, Baba K, Ohta T, and Yamazoe Y (2000) Inhibitory effect of natural furanocoumarins on human microsomal cytochrome P450 3A activity. *Jpn J Pharmacol* **82**:122–129.

Hostetler KA, Wrighton SA, Molowa DT, Thomas PE, Levin W, and Guzelian PS (1989) Coinduction of multiple hepatic cytochrome P-450 proteins and their mRNAs in rats treated with imidazole antimycotic agents. *Mol Pharmacol* **35**:279–285.

Janardan SK, Lown KS, Schmiedlin-Ren P, Thummel KE, and Watkins PB (1996) Selective expression of CYP3A5 and not CYP3A4 in human blood. *Pharmacogenetics* **6**:379–385.

Kawano S, Kamataki T, Yasumori T, Yamazoe Y, and Kato R (1987) Purification of human liver cytochrome P-450 catalyzing testosterone 6β-hydroxylation. *J Biochem (Tokyo)* **102**:493–501.

Kirita S and Matsubara T (1993) cDNA cloning and characterization of a novel member of steroid-induced cytochrome P450 3A in rats. *Arch Biochem Biophys* **307**:253–258.

Kocarek TA, Schuetz EG, Strom SC, Fisher RA, and Guzelian PS (1995) Comparative analysis of cytochrome P4503A induction in primary cultures of rat, rabbit, and human hepatocytes. *Drug Metab Dispos* **23**:415–421.

Kolars JC, Lown KS, Schmiedlin-Ren P, Ghosh M, Fang C, Wrighton SA, Merion RM, and Watkins PB (1994) CYP3A gene expression in human gut epithelium. *Pharmacogenetics* **4**:247–259.

Kolars JC, Schmiedlin-Ren P, Schuetz JD, Fang C, and Watkins PB (1992) Identification of rifampin-inducible P450IIIA4 (CYP3A4) in human small bowel enterocytes. *J Clin Investig* **90**:1871–1878.

Komori M and Oda Y (1994) A major glucocorticoid-inducible P450 in rat liver is not P450 3A1. *J Biochem (Tokyo)* **116**:114–120.

Li AP, Kaminski DL, and Rasmussen A (1995) Substrates of human hepatic cytochrome P450 3A4. *Toxicology* **104**:1–8.

Lowry OH, Rosebrough NJ, Farr AL, and Randall RJ (1951) Protein measurement with the Folin phenol reagent. *J Biol Chem* **193**:265–275.

Marill J, Cresteil T, Lanotte M, and Chabot GG (2000) Identification of human cytochrome P450s involved in the formation of all-*trans*-retinoic acid principal metabolites. *Mol Pharmacol* **58**:1341–1348.

Miyata M, Nagata K, Shimada M, Yamazoe Y, and Kato R (1994) Structure of a gene and cDNA of a major constitutive form of testosterone 6β-hydroxylase (P450/6β A) encoding CYP3A2: comparison of the cDNA with P450PCN2. *Arch Biochem Biophys* **314**:351–359.

Miyata M, Nagata K, Yamazoe Y, and Kato R (1995) Transcriptional elements directing a liver-specific expression of P450/6β A (CYP3A2) gene-encoding testosterone 6β-hydroxylase. *Arch Biochem Biophys* **318**:71–79.

Nagata K, Murayama N, Miyata M, Shimada M, Urahashi A, Yamazoe Y, and Kato

R (1996) Isolation and characterization of a new rat P450 (CYP3A18) cDNA encoding P450(6)β-2 catalyzing testosterone 6β- and 16α-hydroxylations. *Pharmacogenetics* **6**:103–111.

Nagata K, Ogino M, Shimada M, Miyata M, Gonzalez FJ, and Yamazoe Y (1999) Structure and expression of the rat CYP3A1 gene: isolation of the gene (P450/6βB) and characterization of the recombinant protein. *Arch Biochem Biophys* **362**:242–253.

Nelson DR, Koymans L, Kamataki T, Stegeman JJ, Feyereisen R, Waxman DJ, Waterman MR, Gotoh O, Coon MJ, Estabrook RW, et al. (1996) P450 superfamily: update on new sequences, gene mapping, accession numbers and nomenclature. *Pharmacogenetics* **6**:1–42.

Omura T and Sato R (1964) The carbon monoxide-binding pigment of liver microsomes. I. Evidence for its hemoprotein nature. *J Biol Chem* **239**:2370–2378.

Robertson GR, Farrell GC, and Liddle C (1998) Sexually dimorphic expression of rat CYP3A9 and CYP3A18 genes is regulated by growth hormone. *Biochem Biophys Res Commun* **242**:57–60.

Schenkman JB and Jansson I (2003) The many roles of cytochrome b_5. *Pharmacol Ther* **97**:139–152.

Schmiedlin-Ren P, Thummel KE, Fisher JM, Paine MF, and Watkins PB (2001) Induction of CYP3A4 by 1α,25-dihydroxyvitamin D3 is human cell line-specific and is unlikely to involve pregnane X receptor. *Drug Metab Dispos* **29**:1446–1453.

Sempoux C, Starkel P, Stevens M, Van Den Berge V, and Horsmans Y (1999) Cytochrome P450 3A proteins are expressed in B lymphocytes but not in T lymphocytes. *Pharmacogenetics* **9**:263–265.

Strotkamp D, Roos PH, and Hanstein WG (1995) A novel CYP3 gene from female rats. *Biochim Biophys Acta* **1260**:341–344.

Wang H, Kawashima H, and Strobel HW (1996) cDNA cloning of a novel CYP3A from rat brain. *Biochem Biophys Res Commun* **221**:157–162.

Wang H and Strobel HW (1997) Regulation of CYP3A9 gene expression by estrogen and catalytic studies using cytochrome P450 3A9 expressed in *Escherichia coli*. *Arch Biochem Biophys* **344**:365–372.

Waxman DJ, Attisano C, Guengerich FP, and Lapenson DP (1988) Human liver microsomal steroid metabolism: identification of the major microsomal steroid hormone 6β-hydroxylase cytochrome P-450 enzyme. *Arch Biochem Biophys* **263**: 424–436.

Yamazoe Y, Murayama N, Shimada M, Yamauchi K, Nagata K, Imaoka S, Funae Y, and Kato R (1988) A sex-specific form of cytochrome P-450 catalyzing proposycoumarin *O*-depropylation and its identity with testosterone 6β-hydroxylase in untreated rat livers: reconstitution of the activity with microsomal lipids. *J Biochem (Tokyo)* **104**:785–790.

Yamazoe Y, Shimada M, Kamataki T, and Kato R (1986) Effects of hypophysectomy and growth hormone treatment on sex-specific forms of cytochrome P-450 in relation to drug and steroid metabolisms in rat liver microsomes. *Jpn J Pharmacol* **42**:371–382.

Zhang QY, Dunbar D, Ostrowska A, Zeisloft S, Yang J, and Kaminsky LS (1999) Characterization of human small intestinal cytochromes P-450. *Drug Metab Dispos* **27**:804–809.

Address correspondence to: Kiyoshi Nagata, Division of Drug Metabolism and Molecular Toxicology, Graduate School of Pharmaceutical Sciences, Tohoku University, Sendai, 980-8578, Japan. E-mail: nagataki@mail.tains.tohoku.ac.jp

0022-3565/05/3122-759–766
THE JOURNAL OF PHARMACOLOGY AND EXPERIMENTAL THERAPEUTICS
U.S. Government work not protected by U.S. copyright
JPET 312:759–766, 2005

Vol. 312, No. 2
76158/1187717
Printed in U.S.A.

Role of Farnesoid X Receptor in the Enhancement of Canalicular Bile Acid Output and Excretion of Unconjugated Bile Acids: A Mechanism for Protection against Cholic Acid-Induced Liver Toxicity

Masaaki Miyata, Aki Tozawa, Hijiri Otsuka, Toshifumi Nakamura, Kiyoshi Nagata, Frank J. Gonzalez, and Yasushi Yamazoe

Division of Drug Metabolism and Molecular Toxicology, Graduate School of Pharmaceutical Sciences, Tohoku University, Sendai, Japan (M.M., A.T., T.N., H.O., K.N., Y.Y.); and Laboratory of Metabolism, National Cancer Institute, National Institutes of Health, Bethesda, Maryland (F.J.G.)

Received August 12, 2004; accepted September 30, 2004

ABSTRACT

Mice lacking the farnesoid X receptor (FXR) involved in the maintenance of hepatic bile acid levels are highly sensitive to cholic acid-induced liver toxicity. Serum aspartate aminotransferase (AST) activity was elevated 15.7-fold after feeding a 0.25% cholic acid diet, whereas only slight increases in serum AST (1.7- and 2.5-fold) were observed in wild-type mice fed 0.25 and 1% cholic acid diet, respectively. Bile salt export pump mRNA and protein levels were increased in wild-type mice fed 1% cholic acid diet (2.1- and 3.0-fold) but were decreased in FXR-null mice fed 0.25% cholic acid diet. The bile acid output rate was 2.0- and 3.7-fold higher after feeding of 0.25 and 1.0% cholic acid diet in wild-type mice, respectively. On the other hand, no significant increase in bile acid output rate was observed in FXR-null mice fed 0.25% cholic acid diet in contrast to a significant decrease observed in mice fed a 1.0% cholic acid diet in spite of the markedly higher levels of hepatic tauro-conjugated bile acids. Unconjugated cholic acid was not detected in the bile of wild-type mice fed a control diet, but it was readily detected in wild-type mice fed 1% cholic acid diet. The ratio of biliary unconjugated cholic acid to total cholic acid (unconjugated cholic acid and tauro-conjugated cholic acid) reached 30% under conditions of hepatic taurine depletion. These results suggest that the cholic acid-induced enhancement of canalicular bile acid output rates and excretion of unconjugated bile acids are involved in adaptive responses for prevention of cholic acid-induced toxicity.

Hepatic bile acid levels are tightly regulated through manipulation of canalicular output, basolateral uptake, and biosynthesis. Bile salt export pump (Bsep), a bile canalicular ATP-binding cassette transporter, mediates canalicular bile acid excretion. Drugs causing intrahepatic cholestasis, such as cyclosporine A, rifampicin, and glibenclamide, are known to inhibit Bsep/BSEP-mediated taurocholate transport (Stieger et al., 2000; Byrne et al., 2002; Noe et al., 2002). Bsep-null mice exhibit decreased levels of total bile acid output (30% of wild-type mice). Thus, the canalicular bile acid secretion through Bsep is believed to be one of the determinants for maintenance of hepatic bile acid homeostasis. Furthermore, bile acid synthesis and hepatic bile acid uptake from plasma involving cholesterol 7α-hydroxylase (CYP7A1) and Na^+-taurocholate cotransporting polypeptide (NTCP), respectively, might also control homeostasis.

Unconjugated bile acids are conjugated with amino acids in the liver by bile acid-CoA synthetase (BACS) and bile acid-CoA:amino acid *N*-acyltransferase (BAT) before secretion into bile (Schersten et al., 1967; Czuba and Vessey, 1981; Solaas et al., 2000). The bile acids are converted into tauro- or glyco-conjugated forms in humans and almost exclusively to tauro-conjugated forms in mice (Falany et al., 1997). The ATP binding cassette transporter Bsep transports conjugated bile acids into the bile. However, transport of unconjugated bile acids such as cholic acid has not been detected in rodent and humans Bsep-expressing cell lines (Gerloff et al.,

This study was supported by a grant-in-aid from the Ministry of Health, Labor and Welfare.
Article, publication date, and citation information can be found at http://jpet.aspetjournals.org.
doi:10.1124/jpet.104.076158.

ABBREVIATIONS: Bsep, bile salt export pump; CYP7A1, cholesterol 7α-hydroxylase; NTCP, Na^+-taurocholate cotransporting polypeptide; BACS, bile acid-CoA synthetase; BAT, bile acid-CoA:amino acid *N*-acyltransferase; FXR, farnesoid X receptor; PXR, pregnane X receptor; HPLC, high-performance liquid chromatography; RT-PCR, reverse transcription-polymerase chain reaction; AST, aspartate aminotransferase; ALP, alkaline phosphatase; bp, base pair(s); PCR, polymerase chain reaction.

1998; Byrne et al., 2002; Noe et al., 2002). In humans, unconjugated bile acid are almost nondetectable in normal bile (Bjorkhem, 1985).

Recent studies demonstrated that bile acids activate nuclear receptors and regulate transport and biosynthesis of bile acids and lipids. Several bile acids such as cholic acid, chenodeoxycholic acid, and lithocholic acid activate the nuclear receptor farnesoid X receptor (FXR, NR1H4) (Makishima et al., 1999; Parks et al., 1999; Wang et al., 1999). FXR negatively regulates the expression of CYP7A1 and NTCP through induction of small heterodimer partner (NR0B2) while positively regulating the expression of Bsep (Chiang et al., 2000; Goodwin et al., 2000; Lu et al., 2000; Repa et al., 2000; Ananthanarayanan et al., 2001; Denson et al., 2001). Furthermore, several lines of evidence indicate that nuclear receptors other than FXR such as pregnane X receptor (PXR, NR1I2) and vitamin D receptor (NR1I1) are also activated by bile acids (Staudinger et al., 2001; Xie et al., 2001; Makishima et al., 2002).

Bile acid secretion across the hepatic canalicular membrane is generally considered to be the rate-limiting step of the enterohepatic circulation. The bile acid concentrations in serum and liver are indicative of the efficiency of the canalicular secretion. We previously demonstrated that FXR-null mice fed a diet supplemented with 1% cholic acid exhibited severe wasting and hypothermia, resulting in ~30% mortality of the null mice by 7 days, whereas the wild-type mice displayed no overt toxicity (Sinal et al., 2000). To explore the FXR-dependent protective mechanism for cholic acid-induced toxicity, the present study focused on bile acid excretion capacity. The results show a role for cholic acid-induced increase in biliary bile acid output and excretion of unconjugated bile acids in protection against cholic acid-induced toxicity.

Materials and Methods

Materials. Cholic acid, deoxycholic acid, taurocholic acid, taurochenodeoxycholic acid, and taurodeoxycholic acid were purchased from Sigma-Aldrich (St. Louis, MO). HPLC column, Chemcosorb 5-ODS-H (6.0 × 150 mm) was purchased from Chemco Scientific Co. (Tokyo, Japan). L-column ODS (2.1 × 150 mm) was obtained from Kagakuhinnkennsakyoukai (Tokyo, Japan). Enzymepak 3α-HSD column was purchased from Jasco (Tokyo, Japan). Hyodeoxycholic acid and murideoxycholic acid were purchased from Steraloids (Newport, RI).

Animal Treatment and Sample Collection. FXR-null mice (Sinal et al., 2000) were housed under standard 12-h light/12-h dark cycle. Before the administration of special diets, mice were fed standard rodent chow (CE-2; CLEA, Tokyo, Japan) and water ad libitum for acclimation. Experimental diets contained 0.1, 0.25, 0.5, or 1.0% (w/w) cholic acid mixed with the control diet (CE-2). Age matched groups of 8- to 12-week-old animals were used for all experiments and were allowed access to water ad libitum. Bile, blood, and tissue samples were taken for biochemical assays after 5 days of feeding special diets. Total RNA was prepared from livers using the ULTRASPEC II RNA isolation system (Biotecx Laboratories, Houston, TX), and RNA concentrations were determined by measuring the absorbance at 260 nm using a spectrophotometer (Beckman DU 640). Biliary excretion was monitored in anesthetized mice with ethyl ether. After ligation of the common bile duct, the gall bladder was cannulated with a polyethylene-10 tube with an internal diameter of 0.28 mm. The cannula was ligated into the gall bladder to obtain bile samples. After a 5-min equilibration period, bile was collected for 30 min.

Serum AST and Alkaline Phosphatase (ALP) Activities and Determination of Bile Acid. Serum AST activity was estimated by the POP-TOOS [pyruvate oxidase-*N*-ethyl-*N*-(2-hydroxy-3-sulfopropyl)-*m*-toluidine] method using a commercial kit, Transaminase CII-B-test Wako (Wako Pure Chemicals, Osaka, Japan). Serum ALP activity was estimated by the Bessey-Lowry method using Alkaliphospha B-test Wako (Wako Pure Chemicals). Bile, liver, and serum 3α-hydroxy bile acid concentrations were estimated by an enzymecolorimetric method using the Total bile acid-test kit (Wako Pure Chemicals). The liver 3α-hydroxy bile acid contents were measured by HPLC as described previously (Kitada et al., 2003). A portion (100 μl) of liver homogenate was mixed with 1 ml of ethanol containing 2 nmol of androstandiol and treated at 85°C for 1 min, and then centrifuged at 1000*g* for 5 min. After the supernatant was isolated, the precipitate was extracted twice with 1 ml of ethanol and combined extracts were dried and redissolved in 200 μl of methanol. HPLC analyses were performed with a Jasco intelligent model PU-980 pump (Jasco), Waters M-45 pump (Waters, Milford, MA), and FP-920S fluorescence detector (Jasco). The bile acid extracts were separated at 35°C with an L-column ODS (2.1 × 150 mm) (Kagakuhinnkennsakyoukai). The eluates were mixed with a NAD^+ solution before introduction of 3α-hydroxysteroid dehydrogenase immobilized on Enzymepak 3α-HSD column. NADH produced was measured by fluorescence using an excitation wavelength of 365 nm and an emission wavelength of 470 nm. The separation was started at 0.5 ml/min with a 60-min linear gradient of solution A/solution B mixture (25:75) to solution A/solution B mixture (55:45), and then continued with solution A/solution B mixture (55:45) for 25 min [solution A: 10 mM phosphate buffer (pH 7.2)/acetonitrile (60:40); and solution B: 30 mM phosphate buffer (pH 7.2)/acetonitrile (80:20)]. The eluates were passed through a 3α-HSD column after mixing with solution C (1:1) [solution C: 10 mM phosphate buffer (pH 7.2), 1 mM EDTA, 0.05% 2-mercaptoethanol, and 0.3 mM NAD^+].

Hepatic ATP and Taurine Levels. Hepatic ATP levels were measured by the luciferase assay (Lundin and Thore, 1975) using a commercial kit, ATP Assay System LL-100-1 (Toyo Ink, Tokyo, Japan). Hepatic taurine levels were determined by an HPLC method with fluorimetric detection (Waterfield, 1994). Taurine was derivatized with *o*-phthalaldehyde (Sigma-Aldrich) before injection onto COSMOSIL C18 Econopak.

Immunoblot Analysis. Mouse Bsep cDNA containing carboxy terminal region (bp 3195–4070 in AF133903) was subcloned into a prokaryotic expression vector, pQE30 (QIAGEN, Valencia, CA). Recombinant proteins were expressed in *Escherichia coli*, M15 (pREP4) strain, and purified by SDS-polyacrylamide gel electrophoresis. Japanese white rabbits were immunized twice by intradermal injection of 100 μg of the purified protein. Antisera were obtained 1 week after the boost. Specific IgG was purified by affinity column chromatography with Sepharose 4B-bound purified Bsep protein. Crude membranes were prepared from livers by a modification of the method described by Lee et al. (1993). Liver was homogenized in buffer A (100 mM Tris, 100 mM potassium chloride, and 1 mM EDTA) with a protease inhibitor cocktail (20 μM butylated hydroxytoluene and 2 mM phenylmethylsulfonyl fluoride). Nuclei and cell debris were removed by centrifugation at 1000*g* for 15 min. The supernatant was spun at 10,000*g* for 5 min, and the resulting pellet was resuspended in membrane storage buffer (100 mM potassium phosphate, pH 7.4, 1. 0 mM EDTA, 20% glycerol, 1 mM dithiothreitol, and the protease inhibitor cocktail). The crude membrane proteins were loaded onto a 6% polyacrylamide gel, isolated, and transferred to nitrocellulose filters. The filter was immunostained with anti-Bsep IgG (1:1000 dilution), alkaline phosphatase-conjugated goat anti-rabbit IgG (1:3000 dilution), 5-bromo-4-chloro-3-indolylphosphate, and nitro blue tetrazonium as described previously; Honma et al., 2002).

Analysis of mRNA Levels. Messenger RNA levels of differentially expressed genes were analyzed using reverse transcription-polymerase chain reaction (RT-PCR). Single-strand cDNAs were constructed using an oligo(dT) primer with the Ready-to-Go You-Prime First-strand

Beads kit (Amersham Biosciences AB, Uppsala, Sweden). These cDNAs provided templates for PCRs using specific primers at a denaturation temperature of 94°C for 30 s, an annealing temperature of 58°C for 30 s, and an elongation temperature of 72°C for 30 s in the presence of deoxynucleoside-5'-triphosphates and *Taq* polymerase. The PCR cycle numbers were titrated for each primer pair to ensure amplification in linear range. The reaction was completed by a 7-min incubation at 72°C. PCR products were analyzed in 2% agarose gel (w/v) containing ethidium bromide for visualization. The specific forward and reversal primers for the genes examined by PCR were the following: Bsep (bp 2094–2517 in AF133903) sense, 5'-ACAGCATTACAGCTCATTCA-GAG-3', and antisense, 5'-TCCATGCTCAAAGCCAATGATCA-3'; Ntcp (bp 71–671 in U95131) sense, 5'-ACACTGCGCTCAGCGTCATTC-3', and antisense, 5'-GCCAGTAAGTGTGGTGTCATG-3'; Mrp2 (bp 386–1022 in NM 013806) sense, 5'-GGTTCCTGTCCATGTTCTGGATT-3', and antisense, 5'-GCAGCTGAGGATTCAGAAACAAA-3'; Oatp1 (bp 711-1036 in AF148218) sense, 5'-TGATACACGCTGGGTCG-GTG-3', and antisense, 5'-GCTGCTCCAGGTATTTGGGC-3'; BAT (bp 222–713 in U95215) sense, 5'-TCTTGTTGATGAGCCT-GTGC-3' and antisense, 5'-AACTCCATCAATCCACCAGC-3'; BACS sense, 5'-ACCCTGGATCAGCTCCTGGAT-3' and antisense, 5'-GTTCTCAGCTAGCAGCTTGG-3'; taurine transporter (bp 347–807 in NM_009320) sense, 5'-CTTGGAGGTCATCATAGGCC-3' and antisense, 5'-CGGTGAAGTAGACAACCTTGC-3'; Cyp7a1 (bp 119–701 in NM_007824) sense, 5'-CATACCTGGGCTGTGCTCTGA-3' and antisense, 5'-GCTTTATGTGCGGTCTTGAGC-3'; and GAPDH (bp 487–1018 in NM_008084) sense, 5'-TGCATCCTGCACCACCAACTG-3', and antisense, 5'-GTCCACCACCCTGTTGCTGTAG-3'. To more precisely quantify Bsep mRNA level, real-time PCR was carried out with SYBR Green by using ABI PRISM 7000 (Applied Biosystems, Foster City, CA). To calculate Bsep mRNA level, a standard curve was generated by plotting the threshold cycle value versus the log of the amount of mouse Bsep cDNA. Bsep mRNA levels were normalized from the GAPDH mRNA levels.

Results

Cholic Acid-Induced Liver Damage and Hepatic Bile Acids. Under control diet feeding, serum AST activity was 2.6-fold higher in FXR-null mice than in the wild-type mice. No significant difference in serum ALP activity was observed between both lines of mice (Table 1). Because FXR-null mice exhibited some mortality during 1% cholic acid feeding for 5 days, the mice were thereafter fed a 0.25% cholic acid diet in the present study. Serum ALP activity was increased to 4.9-fold in FXR-null mice fed a 0.25% cholic acid diet, whereas the increase was minimal (1.6-fold) in the wild-type mice even after a 1.0% cholic acid diet. Serum AST activity increased 15.7-fold in FXR-null mice fed a 0.25% cholic acid diet, compared with the mice fed a control diet. Slight increases (1.7- and 2.5-fold) were observed in wild-type mice fed either 0.25 or 1.0% cholic acid diets.

Feeding 0.25% cholic acid diets resulted in clear increases in serum and hepatic bile acid levels in FXR-null mice. Similar experiments on wild-type mice revealed only slight increases in hepatic bile acid levels and no significant increases in the serum bile acid level. A significant correlation (r^2 = 0.92) was observed between hepatic bile acid concentrations and AST activity in individual mice (Fig. 1).

Bile Salt Export Pump Protein and mRNA Levels. Decreased levels of canalicular bile acid transporter, Bsep represents one possible mechanism for cholestasis. Changes in hepatic mRNA levels of Bsep were assessed in cholic acid-fed mice by RT-PCR (Fig. 2A). The mRNA levels were increased in the wild-type mice fed cholic acid diet. In contrast, no clear increase in the Bsep mRNA levels was observed in FXR-null mice after feeding 0.25% cholic acid diet. Furthermore, hepatic mRNA levels of Bsep were quantified by real-time PCR revealing 2.0-fold higher levels of specific Bsep mRNA in control diet-fed wild-type mice compared with control diet-fed FXR-null mice (Fig. 2B). Bsep mRNA levels became 2.1-fold higher in wild-type mice after 1.0% cholic acid feeding. Consistent with Bsep mRNA levels, Bsep protein levels assessed by immunoblotting were higher in the wild-type mice fed control diets than in FXR-null mice and became 3.0-fold higher in wild-type mice after 1.0% cholic acid feeding (Fig. 2C), whereas no significant increases in protein levels were found in FXR-null mice fed 0.25 and 1.0% cholic acid diets and in wild-type mice fed 0.1 and 0.5% cholic acid diet (data not shown).

Bile Flow and Bile Acid Output Rate. Bile acid secretion across the canalicular membrane is the rate-limiting step of enterohepatic circulation under normal dietary conditions. Bile flow and bile acid output rate (3α-hydroxy bile acid excretion rate), which correlate with bile acid excretion rates to the bile duct, were determined in both mice fed a control diet or a cholic acid diet, to determine the biliary excretion capacity (Fig. 3, A and B). Contrary to the Bsep protein levels, bile acid output rate was significantly higher in FXR-null mice fed control diets than that in the wild-type mice (Fig. 3B). Hepatic bile acid concentrations were 2.5-fold higher in FXR-null mice than that in the wild-type controls. An increase in bile acid output rate and hepatic bile acid concentration was observed in the wild-type mice fed the cholic acid diet. Feeding a 1% cholic acid diet to wild-type mice increased the bile flow and bile acid output rate by 3- and 3.7-fold, respectively. In FXR-null mice, no significant difference in bile flow and bile acid output rate was observed between control diet and cholic acid (0.1 and 0.25%) diet in spite of the marked accumulation of hepatic bile acids (2.0 μmol/g liver) in FXR-null mice fed 0.25% CA diet (Fig. 3B). Furthermore, a decrease in bile flow and bile acid output

TABLE 1

Liver diagnostic markers and levels of 3α-hydroxy bile acid

Control or cholic acid-supplemented diets were given for 5 days to wild-type and FXR-null male mice. The data are shown as the mean ± S.D. (n = 4–6).

Parameters	Wild-Type Mice				FXR-Null Mice		
	Control	0.25%	0.5%	1.0%	Control	0.1%	0.25%
Serum 3α-OH bile acid (μM)	5 ± 2	8 ± 5	127 ± 50[a]	412 ± 261[b]	9 ± 2	13 ± 3	316 ± 136[b]
Liver 3α-OH bile acid (nmol/g liver)	147 ± 35	206 ± 35[a]	318 ± 95[a]	1231 ± 282[b]	372 ± 141	657 ± 121[a]	2742 ± 670[b]
AST activity (IU/l)	23 ± 5	40 ± 12[a]	36 ± 14	55 ± 5[a]	59 ± 18	ND	929 ± 325[b]
ALP activity (IU/l)	28 ± 1	22 ± 5	32 ± 13	44 ± 10[a]	24 ± 1	22 ± 6	117 ± 52[a]

3α-OH, 3α-hydroxy; ND, not determined.
[a] $p < 0.05$ versus control.
[b] $p < 0.01$ versus control.